Ph.D. DISSERTATION

Fabrication and Performance of Liquid Crystal Polymer (LCP)-based Neural Probes: Four-sided Probe and Optrode

액정폴리머기반의 신경 전극의 제작과 성과:

사면 전극과 옵트로드

BY

SOOWON SHIN

AUGUST 2017

DEPARTMENT OF ELECTRICAL ENGINEERING AND COMPUTER SCIENCE
COLLEGE OF ENGINEERING
SEOUL NATIONAL UNIVERSITY

Fabrication and Performance of Liquid Crystal Polymer (LCP)-based Neural Probes: Four-sided Probe and Optrode

지도 교수 김 성 준

이 논문을 공학박사 학위논문으로 제출함

2017년 8월

서울대학교 대학원

전기·컴퓨터공학부

신 수 원

신수원의 공학박사 학위논문을 인준함

2017년 8월

위 원 장 이 종 호 (인)

부위원장 김 성 준 (인)

위 원 서 종 모 (인)

위 원 김 성 재 (인)

위 원 이 승 희 (인)

Abstract

A novel liquid-crystal polymer (LCP)-based neural probe with four-sided electrode sites is developed. Ideally, neural probes should have channels with a three-dimensional (3-D) configuration to record 3-D neural circuits. Many types of three-dimensional neural probes have been developed; however, most of them were formulated as an array of multiple shanks with electrode sites located along one side of the shanks. The proposed LCP-based neural probe has electrode sites on four sides of the shank, i.e., the front, back and two side walls. To generate the suggested configuration of the electrode sites, a thermal lamination process involving LCP films and laser micromachining are used. Using the proposed novel four-sided neural probe, *in vivo* multichannel neural recording is successfully performed in the mouse primary somatosensory cortex. The multichannel neural recording shows that the proposed four-sided neural probe can record spiking activities from a diverse neuronal population compared to neural probes with single-sided electrodes. This is confirmed by a pair-wise Pearson correlation coefficient (Pearson's r) analysis and a cross- correlation analysis.

This study also presents the development of LCP-based depth-type stimulation electrodes with a high charge storage capacity using electrodeposited iridium oxide film (EIROF). On the electrode sites, iridium oxide is

electrodeposited to increase the charge storage capacity for facilitating neural stimulation. After electrodeposition using different numbers of rectangular voltage pulses and triangular waveforms, the iridium oxide electrodes are characterized in terms of charge storage capacity and electrochemical impedance. And the surfaces of EIROFs are examined using atomic force microscopy (AFM) and scanning electron microscopy (SEM). In addition, the elementary composition of the EIROF surfaces is quantitatively determined using X-ray photoelectron spectroscopy (XPS). The *in vivo* neural experiments verified the feasibility of the proposed LCP-based depth-type stimulation electrode.

Additionally, LCP-based optrode is suggested for optical stimulation and electrical recording. The suggested neural probes have four contacts at the tip of the electrode shank. After thermally laminating the LCP films, the four tip electrodes are made by cut-exposing the thickness of the electroplated metals. The four tip electrodes have enough contact areas and electrochemical impedance to ensure good quality of neural signal recordings. After the laser cutting process, an optic fiber is integrated to the neural probes. To demonstrate optical stimulation and electrical recording capability of the fabricated LCP-based optrode, *in vivo* experiments are done. Spontaneous activity and light-evoked activity are successfully recorded from the cortex and the deep brain area.

Keywords: neural probe, liquid crystal polymer, three-dimensional, tetrode, optrode, recording electrode, stimulation electrode, iridium oxide

Student Number: 2013-30244

Contents

List of Figures

List of Tables

List of Abbreviations

Abbreviation	Term
AFM	Atomic Force Microscopy
AIROF	Activated Iridium Oxide Film
CAD	Computer-Aided Design
CSCc	Cathodic Charge Storage Capacity
CV	Cyclic Voltammetry
DBS	Deep Brain Stimulation
EIROF	Electrodeposited Iridium Oxide Film
EIS	Electrochemical Impedance Spectroscopy
ESA	Electrochemical Surface Area
GSA	Geometric Surface Area
ICSS	Intra Cranial Self–Stimulation
LCP	Liquid Crystal Polymer

LFP	Local Field Potential
MFB	Medial Forebrain Bundle

Abbreviation	**Term**
PBS	Phosphate-Buffered Saline
PSTH	Peri-Stimulus Time histogram
S1	Primary Somatosensory Cortex
SD rat	Sprague-Dawley rat
SEM	Scanning Electron Microscope
SIROF	Sputtered Iridium Oxide Film
V1	Primary Visual Cortex
VPL	Ventral Posterolateral Nucleus
XPS	X-ray Photoelectron Spectroscopy

Note

Some parts of this dissertation are extracted and adapted from the journal publications which were published during the course of this study:

- Soowon Shin, Junghoon Kim, Joonsoo Jeong, Tae Mok Gwon, Gwang Jin Choi, Sung Eun Lee, Jinhyung Kim, Sang Beom Jun, Jin Woo Chang, and Sung June Kim, "High Charge Storage Capacity Electrodeposited Iridium Oxide Film on Liquid Crystal Polymer-Based Neural Electrodes," *Sensors and Materials*, 28(3), pp.243-260, 2016.

- Soowon Shin, Jae-Hyun Kim, Joonsoo Jeong, Tae Mok Gwon, Seung-Hee Lee, and Sung June Kim, "Novel four-sided neural probe fabricated by a thermal lamination process of polymer films," *Journal of Neuroscience Methods*, 278, pp.25-35, 2017.

Chapter I

Introduction

1.1 Neural Probes

1.1.1 Recording Probes

For studying the functioning of the brain, it is critical to employ tools that can perform neural recording or stimulate brain tissue. For decades, various implantable neural probes of different shapes and made from different materials have been developed; these probes are capable of single or multiple instances of neural recording or stimulation of brain tissue [1]-[30]. Among them, metal-wire-based neural probes have been used the most to record *in vivo* neural signals [1], [12], [15], [27]. Earlier versions of these metal-wire-based probes had only one recording site at the tip of the wire. Later versions of the probes were developed by assembling a bundle of wires to increase the number of electrodes, but such attempts increased the cross-sectional area of the probe, which increased the possibility of causing undesirable damage to brain tissue during the insertion of the probe [6], [12], [15], [16], [27]. Improvements in micro-fabrication technologies over the past several decades have allowed researchers to produce multi-channel neural recording probes using silicon as the substrate material [2]-[5], [8], [9], [13], [14], [17], [18], [20]-[22], [26], [28], [30]. Micro-fabricated neural probes have the advantage of reproducibility, and they can be created with multiple electrodes without increasing the size of the probe. However, the mechanical brittleness of silicon poses the risk of breakage during the probe handling and insertion processes [16]. Recently, polymers such as polyimide, parylene, and liquid crystal polymer (LCP) have been highlighted as possible materials for neural probes owing to their

good flexibility and compatibility with semiconductor fabrication processes [7], [10], [11], [19], [23], [24], [29]. However, due to their shortcoming of insertion rigidity, polyimide- and parylene-based neural probes require additional reinforcements of in their structures to support the insertion of flexible probes into the brain [10], [11], [16], [23], [29]. In addition, ceramics have been used as the substrate material for neural probes and additional reinforcements to achieve insertion rigidity [23] [25].

To stimulate or record from complex neural circuits or record their activities, neural probes with high-density electrodes in a three-dimensional (3-D) configuration have been widely used. Many types of 3-D neural probes with multiple channels and multiple shanks have been developed using silicon and polymers through micro-fabrication processes [2]-[5], [7]-[11], [13], [14], [16]-[26], [28]-[30]. Among them, silicon-based multichannel neural probes have been fabricated with small thicknesses and average widths of 100 μm, with 4 to 188 channels per shank and with a high degree of integration [2]-[5], [8], [9], [13], [14], [17], [18], [20]-[22], [26], [28], [30]. However, most of these probes have similar structures in which the electrodes are located along one side of the shanks. Although there has been an attempt to fabricate a parylene-based neural probe with three-sided electrode contacts, additional processes were needed to prevent the delamination of the parylene-C layers [19].

1.1.2 Stimulation Electrodes

Neural prostheses use electrical stimulation for restoration and control of the

nervous system. For instance, cochlear implants and retinal implants deliver electrical stimulations to the neural pathways of people with auditory and visual impairments, respectively [31-36]. Deep brain stimulation (DBS) also uses electrical stimulation to treat neuropathic disorders such as Parkinson's disease, epileptic seizures, and neuropathic pain [24], [37]-[43].

Various materials have been tried as stimulation electrode materials for neural prostheses, such as platinum, gold, iridium oxide, poly (3,4-ethylenedioxythiophene):PEDOT, and titanium nitride [44]. Noble metals such as platinum and gold have been widely used for electrode sites due to their high durability. However, microelectrodes with noble metals have insufficient charge-injection capacities for stimulation. Therefore, in order to increase the charge-injection capacity, materials with specific surface structures or with electrochemically non-polarizable characteristics have been developed, such as titanium nitride, PEDOT, and iridium oxide. The high charge-injection capacities of these materials are obtained due to their high surface roughness characteristics, making their electrochemical surface area (ESA) much higher than the geometric surface area (GSA). Titanium nitride is a capacitive charge-injection material, which is more desirable than faradaic charge-injection materials because it creates or consumes no chemical species during stimulation. Moreover, the conductive polymer known as PEDOT, which delivers charges in a faradaic manner, has recently been studied as an alternative. Among the various materials, iridium oxide films have attracted significant attention from researchers due to their extraordinarily high charge-injection capacities. Iridium oxide has a high charge-

injection capacity due to the reversible faradaic reactions it undergoes, involving reduction and oxidation processes between Ir^{3+} and Ir^{4+}.

In order to form iridium oxide electrodes, various methods have been attempted, such as sputtering, activation, and electrodeposition. Sputtered iridium oxide film (SIROF) is formed by DC reactive sputtering using an iridium metal target under oxidizing plasma conditions [45]-[49]. Activated iridium oxide film (AIROF) can be formed via an activation process in an aqueous electrolyte using iridium wires or sputtered iridium films. The activation is an oxidative process from iridium to iridium oxide by means of cycling between negative and positive potentials within the potential limits of water electrolysis [36], [50]-[52]. Electrodeposited iridium oxide film (EIROF) can be directly deposited from an iridium salt solution using pulsed voltage, DC voltage, or cyclic voltammetry [53]-[57].

The different fabrication processes for iridium oxide film show different characteristics in terms of durability, fabrication complexity, or fabrication compatibility. For example, it was reported that AIROFs can be delaminated from an underlying iridium layer because uneven growth of the oxide layer introduces strain [48], [58]. In order to deposit SIROFs, in general, the substrate must be heated to a temperature above 400 °C [59]-[61]. However, if the electrode substrate is made of polymers, the elevated temperature during sputtering is not suitable since the polymers are deformed near or above their melting temperature, which is typically around 300 °C. In order to prevent the temperature increase of polymer substrates, intermediate cool-down steps were introduced during sputtering [46].

However, this appeared to cause cracks in the SIROF layers during thermal lamination of LCP layers, which is an indispensable step in making monolithic and implantable neural electrodes from LCP. Unlike the SIROFs, the deposition of EIROFs is compatible with the thermal lamination process because the electrodeposition is generally performed after the fabrication processes are finished.

1.1.3 Optrodes

Neural electrical stimulation has been a powerful tool in electrophysiology and neuroscience [62], [63] despite the lack of spatial selectivity by volume electrical stimulation [64]. Recently, optical stimulation has been widely investigated to selectively stimulate the specific neural cells which are genetically modified to respond to a light illuminated at a specific wavelength [65], called optogenetics. Through modulation by light-sensitive ion-channels, neurons can be optically excited or inhibited as a response to different wavelengths of light stimulation. The excitation or inhibition of neurons can be induced with millisecond time resolution [65]. The advantage of optogenetics is that light-induced modulation can achieve control of one type of cell in the brain while leaving others unaltered and analyze the neural circuit information processes more controllable with higher spatial specificity.

For optogenetic researches, various kinds of optrodes have been constructed to optically stimulate specific cells and electrically record their neural activity. The most widely used optrode in the researches is made by simply gluing an optical fiber to a microwire-based tetrode [66], [67]. Similarly, optrode made of

optical fiber glued onto a multi-site silicon probe has also been made [68], [69]. Another type of optrode is that silicon-based probe with waveguide made on it [70]-[72].

1.2 Proposed Neural Probes

1.2.1 Recording Probes

In this study, the development of recording neural probes with four-sided contacts using LCP is proposed. The use of LCP as the substrate material offers the additional advantage of an adjustable thickness in the range of tens to hundreds of micrometers. The LCP-based neural probes is not fragile and can be inserted into the brain without any insertion guide tool unlike other polymer-based depth-type probes [24]. Moreover, LCP has a lower moisture absorption rate and is less permeable to moisture than other polymers, making it advantageous for neural recording given its long-term durability *in vivo* [33], [46], [73]-[77]. In this study, a novel neural probe with four electrodes on the four sides of the electrode shank, i.e., the front, back and two sidewalls is suggested. This neural probe is fabricated by a micro-fabrication process, a thermal lamination process, and laser micromachining. The proposed novel LCP-based four-sided neural probe, can be used to simultaneously record neural signals from three-dimensionally distributed neuronal ensembles in brain tissue. To show the superiority of the four-sided neural probes over the single-sided neural probes through *in vivo* neural recording experiments, an LCP-based neural probe with single-sided electrodes is also made.

1.2.2 Depth-type Stimulation Electrode

In this study, LCP-based depth-type stimulation electrode with EIROF electrode sites are proposed. These electrodes have the advantages of a LCP substrate and a high charge storage capacity through their use of EIROF electrode sites. The use of EIROFs on LCP was previously mentioned very briefly [54]. In this study, however, a fabrication process for LCP-based neural electrodes establishes with optimized EIROF sites. The EIROFs are electrochemically formed with triangular waveforms and rectangular pulses to increase their adhesive stability and their charge storage capacity, respectively [55]. The characteristics of the fabricated LCP-based flexible neural electrodes with EIROF sites are validated using electrochemical, mechanical, microscopic, and spectroscopic methods. Moreover, *in vivo* neural experiments were done to demonstrate the feasibility of the proposed EIROFs as electrode site materials. Also, LCP-based depth-type stimulation electrode having electrode sites on the front- and back-side and at the tip of the electrode shank is suggested.

1.2.3 Optrode

In this study, LCP-based optrode made with micro-fabricated tetrode using LCP and optic fiber is proposed.

The suggested LCP-based tetrode is designed to have four recording electrodes at the tip of the electrode shank and fabricated by a micro-fabrication process, a thermal lamination process, and a laser micromachining. The

configuration of suggested tetrode mimics that of microwire-based tetrodes, which is widely used in neural recording experiments. The advantage of the microwire-based tetrodes among various neural electrode arrays is that its structure allows electrode sites to have easy access to nearby intact neurons. However, the fabrication process of the microwire-based tetrodes requires a mastery of manual skills and the resulting device tends to be unregulated. Suggested LCP-based tetrode can be manufactured with well controlled dimensions using micro-fabrication while maintaining the structural advantages of the microwire-based tetrode.

The LCP-based optrode is made by integrating optic fiber to the LCP-based tetrode. Therefore, suggested optrode can be applicable to the *in vivo* experiments in the cortex as well as the deep brain area because the optic fiber is integrated into neural probe. Also the structural advantages of the tetrode can be maintained.

1.3 Dissertation Outlines

This dissertation is addressing fabrication and evaluation of LCP-based neural probes

In the chapter 2: Materials and Methods, firstly the substrate material of the neural probes, liquid crystal polymer is introduced in chapter 2.1. Next, electrode configurations of the suggested neural probes are suggested in chapter 2.2. In the following chapter 2.3 and chapter 2.4, micro-fabrication processes and

measurements of electrochemical property of the neural probes are explained. Electrodeposition process of iridium oxide film and its electrochemical and mechanical characteristics are detailed in the chapter 2.5. In chapter 2.6, *in vivo* evaluation experiments of the proposed neural probes are suggested.

The chapter 3: Results show the fabricated neural probes in chapter 3.1 and their measured electrochemical characteristics in chapter 3.2. The characteristics of the fabricated electrodeposited iridium oxide film (EIROF) electrodes are validated in chapter 3.3 using electrochemical, mechanical, microscopic, and spectroscopic methods. The following chapter 3.4 shows the results of *in vivo* evaluation experiments of the developed neural probes.

The chapter 4: Discussion explores the capability of the various neural probes developed in this study and discusses their further development potentialities.

The dissertation is finished with a concluding paragraph for summary and future work in the chapter 5.

Chapter II

Materials & Methods

2.1 Liquid Crystal Polymer (LCP)

Liquid Crystal Polymer (LCP) is biocompatible, flexible, chemically inert, and mechanically stable thermoplastic polymer consisting of rigid and flexible monomers that link to each other as shown in Figure 2.1. LCP has been used for many biomedical applications, including deep-brain stimulation [24], [78], [79]; the development of retinal prostheses [33], [80], [81], and cochlear implants [32], [82], [83]; and intraocular pressure monitoring [81]. Recently, different technologies have been developed for LCP-based neural prostheses, such as the microfabrication of electrodes [24], [32], [33], [46], [74], [78]-[82], [84]; planar coil fabrication [85]; thermal deformation [80], [81]; monolithic encapsulation [75], [81]; and magnetic resonance imaging compatibility [83].

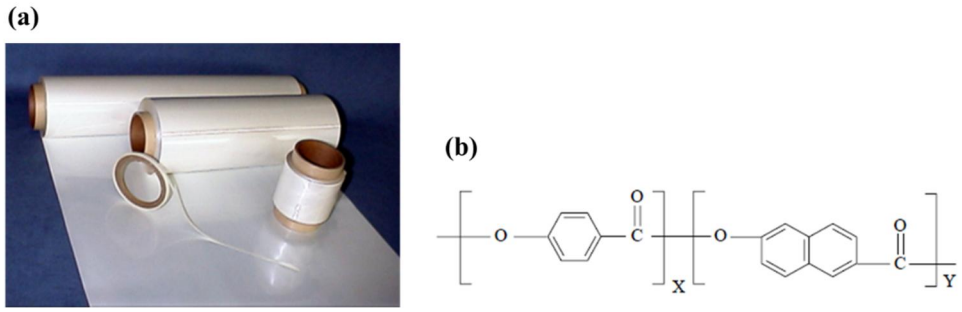

Figure 2.1 (a) Commercial liquid crystal polymer (LCP) film (Vecstar CTF series, Kuraray, Tokyo, Japan). (b) Molecular structure of LCP.

The most important advantage of LCP is that its moisture absorption rate (<0.04%) is lower than those of other biocompatible polymers such as parylene-C (0.06–0.6%) and polyimide (~2.8%); this rate is directly linked to long-term

reliability [33], [46], [73]-[76], [80], [81], [86]-[88]. The long-term reliability of LCP superior to polyimide and parylene-C has been demonstrated by accelerated soak tests [75].

Other important properties of LCP for use in biomedical applications are its compatibility with micro-fabrication processes and its useful thermoplastic characteristics [24], [32], [33], [46], [74], [75], [77]-[82], [84], [85]. LCP is not damaged or dissolved by commonly used chemicals in micro-fabrication processes such as organic solvents (acetone and alcohol), photoresist, photoresist developers/removers and acidic etchants for metals [73], [89]. Therefore, it is possible to form micron-scale metal patterns for the microelectrode array on the LCP film by applying the micro-fabrication processes including spin coating, metallization, photolithography, dry and wet etching. The multiple LCP films having metal patterns thus produced can be thermally laminated together without using any other adhesives due to the thermoplasticity properties of LCP. These properties contribute to not only the creation of monolithic biomedical systems but also the fabrication of the multilayered electrode structure proposed in this study.

2.2 Electrode Configuration

2.2.1 Recording Probes

2.2.1.1 Four-sided Neural Probe

The configuration of the proposed LCP-based neural probe with four-sided electrodes is depicted in Figure 2.2. Four electrodes exist on the four sides of the

shank: the front, back, left, and right sides. The open area of the electrodes on the front and back sides is 40 μm × 40 μm, and the two sidewall electrodes have an open area of 5 μm × 100 μm. The electrode shank has 10 mm length, 350 μm width, and 150 μm thickness.

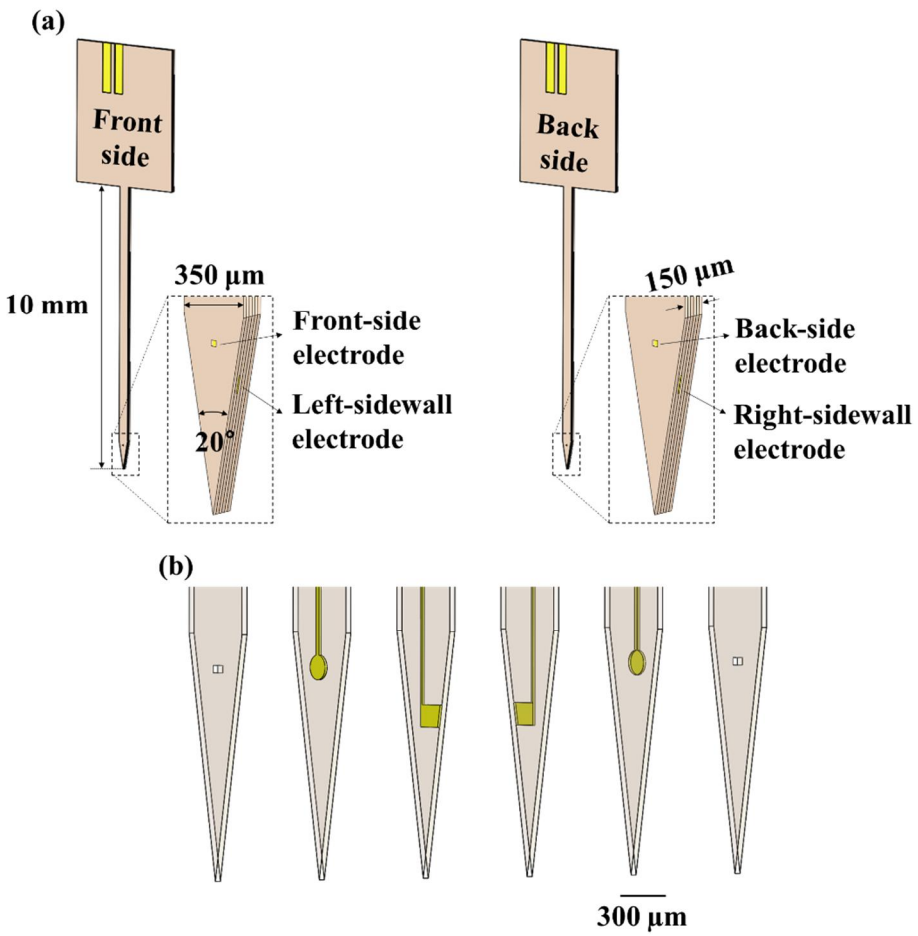

Figure 2.2 (a) LCP-based neural probes with four-sided electrodes: the four electrodes are on the four side of the electrode shank. (b) Detailed LCP layers of the neural probe: front-cover LCP layer, front-side electrode patterned LCP layer, left-sidewall electrode patterned LCP layer, right-sidewall electrode patterned LCP layer, back-side electrode patterned LCP layer, and back-cover LCP layer.

2.2.1.2 Single-sided Neural Probe

The configuration of the proposed LCP-based neural probe with single-sided electrodes is depicted in Figure 2.3. Four electrodes exist on the front side of the electrode shank. The open area of the electrodes is 40 μm × 40 μm. The size of shank is same with four-sided neural probe.

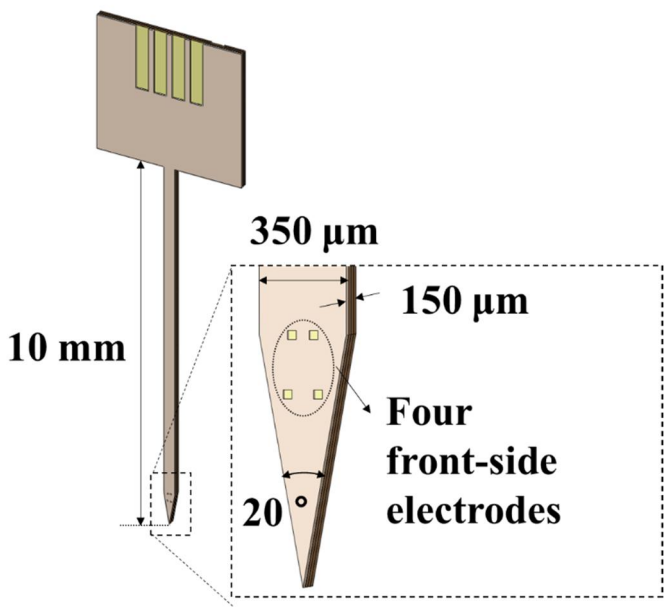

Figure 2.3 LCP-based neural probes with single-sided electrodes: four electrodes are located on the front side of the electrode shank.

2.2.1.3 Tetrode

The configuration of the proposed LCP-based tetrode is depicted in Figure 2.4. The LCP-based tetrode has four electrodes located at the tip of the electrode shank. The open area of the electrodes is 10 μm × 100 μm. The size of shank is same with other suggested recording probes.

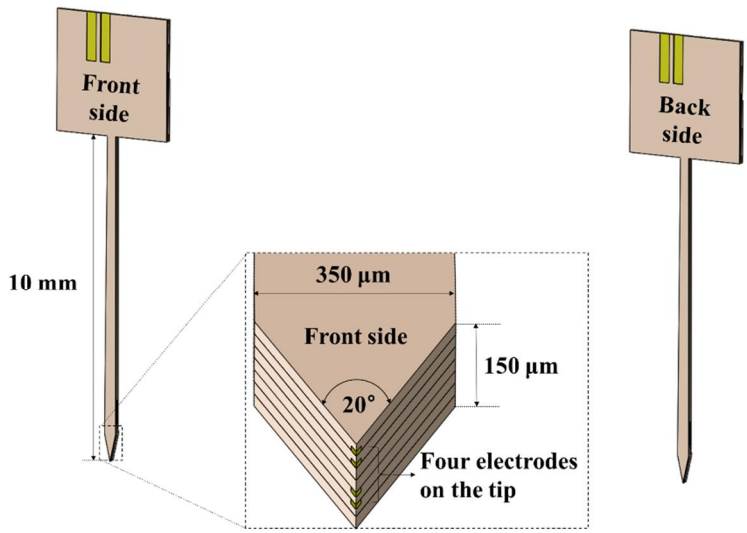

Figure 2.4 LCP-based tetrode: four electrodes are located at the tip of the electrode shank.

2.2.2 Depth-type Stimulation Electrode

The configuration of the proposed LCP-based depth-type stimulation electrode is depicted in Figure 2.5. Suggested stimulation electrode has eight electrodes in total. Three electrodes are located on the front, the other three electrodes are on the back side, and two electrodes are at the tip of the electrode shank. The open area of the electrodes on the front and back sides is 20 µm × 75 µm, and the two tip electrodes have an open area of 10 µm × 150 µm. The electrode shank has 10 mm length, 250 µm width, and 250 µm thickness.

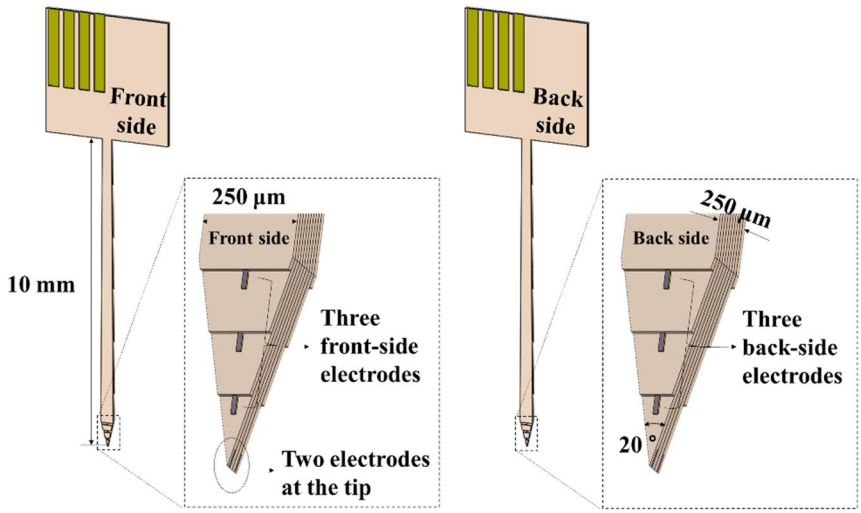

Figure 2.5 LCP-based depth-type stimulation electrode. Eight electrodes are on the front and back side and at the tip of the electrode shank.

2.2.3 Optrode

The configuration of the proposed LCP-based optrode is depicted in Figure 2.6. The LCP-based Optrode has four electrodes located at the tip of the shank. The open area of the electrodes is 10 μm × 100 μm. The electrode shank has 10 mm length, 300 μm width, and 300 μm thickness. An optic fiber is integrated in the suggested LCP-based optrode for optical stimulation.

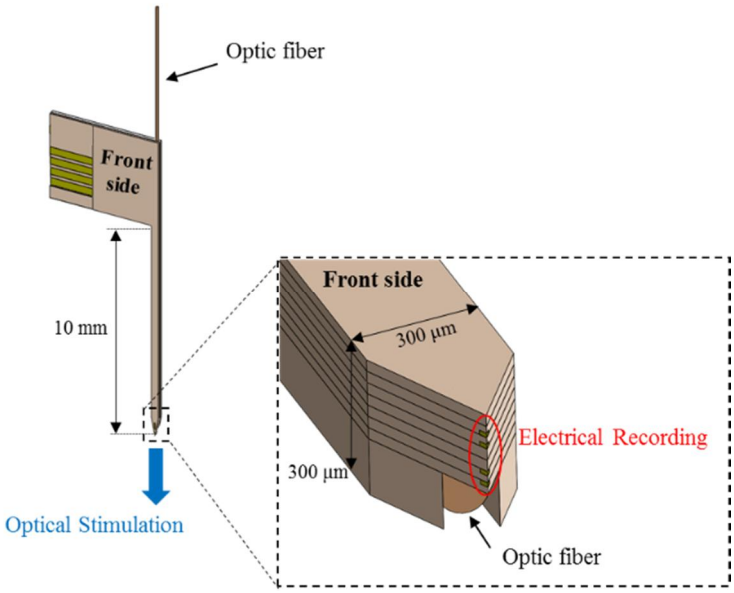

Figure 2.6 LCP-based optrode has four electrodes located at the tip of the electrode shank and integrated optic fiber.

2.3 Fabrication Processes

The fabrication process of the suggested neural probes is based on previously reported LCP fabrication processes [24], [32], [33], [80], [78], [79], [81], [82]. The suggested neural probes are manufactured with same basic fabrication processes. The differences in making each neural probe are discussed after the basic fabrication process description.

An LCP film (Vecstar CTF series, Kuraray, Tokyo, Japan) is fixed on a silicon wafer using silicone elastomer (MED-6233, NuSil Technology, CA, ISA). To clean the surface of the LCP film, it is immersed sequentially in acetone, methanol, isopropyl alcohol, and deionized water for 1 min each. The surface of the LCP film is then activated by oxygen plasma (150 W, 100 sccm, 3 min; Plasmalab

80 plus, Oxford Instruments, U.K.) Subsequently, metal seed layers for the electroplating process—a 50-nm-thick titanium layer and a 150-nm-thick gold layer—, are evaporated using an electron gun (e-gun) evaporator (ZZS550-2/D, Maestech Co., Ltd., Pyungtaek, South Korea). The e-gun evaporation process involves the physical vapor deposition of metal using an electron beam under high vacuum conditions. Next, a photolithography step is carried out using an aligner (MA6/BA6, SUSS MicroTec, Garching, Germany), and gold is electroplated onto the metal seed layers. After electroplating a 5-μm-thick or 10-μm-thick of gold layer, the photomask is removed and the metal seed layers are wet-etched using nitrohydrochloric acid and hydrofluoric acid. The thickness of the electroplated gold and the number of the metal-patterned LCP film depend on which neural probe is made. After the wet-etched process, surface of the metal-patterned LCP films and LCP cover layers is activated by oxygen plasma. The LCP cover layer is a bare LCP film used for the insulation. If necessary, the LCP cover layers can be cut through laser micromachining (Samurai UV Marking System, DPSS Lasers Inc., Santa Clara, CA, USA) before the activation process. Then, the LCP layers with metal patterns and LCP cover layers aligned in a metal jig are laminated together using a thermal press (30 min, 285 °C, 2 kgf/cm^2; Model 4122, Carver, Wabash, IN, USA). After the thermal lamination, the laser ablation and final laser cutting processes are done by means of laser micromachining. Laser ablation creates a window through which the electrode pads and the electrodes on the front and back sides are exposed sequentially. The final laser cutting step not only forms a neural probe outline but also creates the side and tip electrodes by exposing the thickness

of the electroplated metals through cuts.

The fabrication process of the four-sided neural probe is schematically shown in Figure 2.7. To create the four-sided contacts, a photolithography mask with patterns of four sectioned areas; each area has the patterns required to form one side of the four-sided contacts is developed (Figure 2.8). After the wet-etched process, the metal-patterned LCP film is cut into four film pieces, and each cut LCP film has the metal patterns of one of the four-sided contacts. After surface activation by oxygen plasma, the four cut LCP layers with metal patterns and the cover layers aligned in a metal jig are laminated together using a thermal press. In this step, LCP films for the right-sidewall and back-side electrodes are laid on a metal jig upside down, as shown in Figure 2.7 (f). Consequently, the metal patterns of these two layers face the floor, which implies that the electrode pads for the right-sidewall and back-side electrodes are formed on the back side of the neural probe. Laser ablation creates the electrodes on the front and back sides and the final laser cutting step forms right- and left-sidewall electrodes.

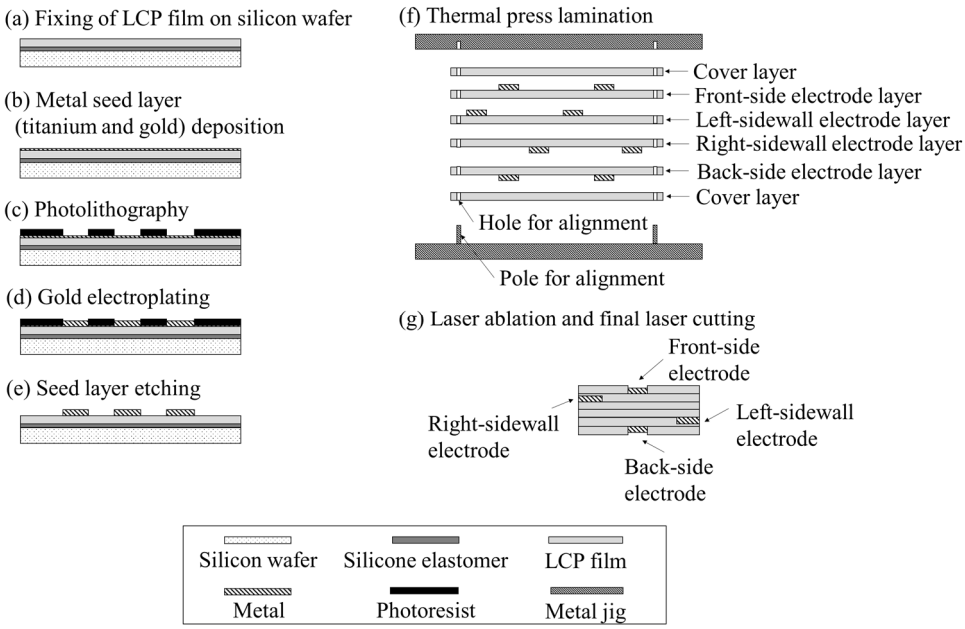

Figure 2.7 Fabrication process of LCP-based neural probe with four-sided electrodes: (a) fixing of an LCP film on a silicon wafer, (b) metal seed layer deposition, (c) photolithography, (d) gold electroplating, (e) metal seed layer wet etching, (f) thermal lamination of multiple LCP films using a metal jig pair, and (g) laser micromachining. Laser ablation opens a window that exposes the electrodes on the front and back sides, and the two sidewall electrodes are exposed during the outline laser cutting process.

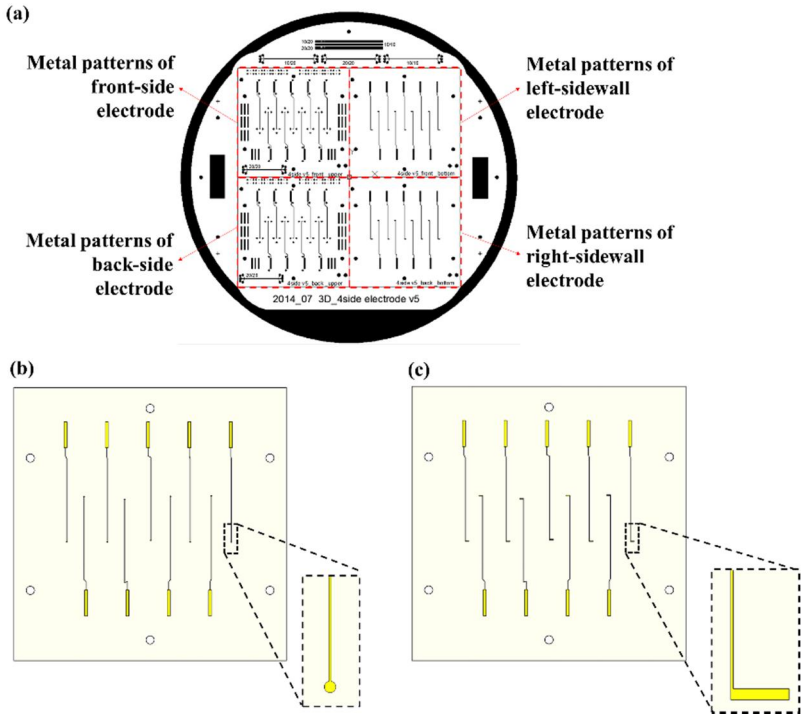

Figure 2.8 (a) CAD drawing of the photolithography mask. The patterns on the mask have four sectioned areas of the four-sided electrodes. (b) Enlarged view of the design of the front- and back-side electrodes. (c) Enlarged view of the design of the left- and right-sidewall electrodes.

To make the LCP-based neural probe for single-sided electrodes, the same fabrication process used with the LCP-based neural probe with the four-sided contacts is used. The only difference between the fabrication processes for the two types of neural probes is the photolithography masks used. When the photolithography mask for the single-sided contacts is used, the metal-patterned LCP layer has patterns that cause single-sided contacts to be formed on the front side of the neural probe. Therefore, the metal-patterned LCP layer formed after the wet-etching process and the cover layer are thermally laminated together. In the last step, laser micromachining is carried out. Laser ablation creates a window that

exposes the electrodes on the front side, and the final laser cutting step is used only for the cutting of the neural probe. The fabrication process of the LCP-based single-sided neural probe is schematically shown in Figure 2.9.

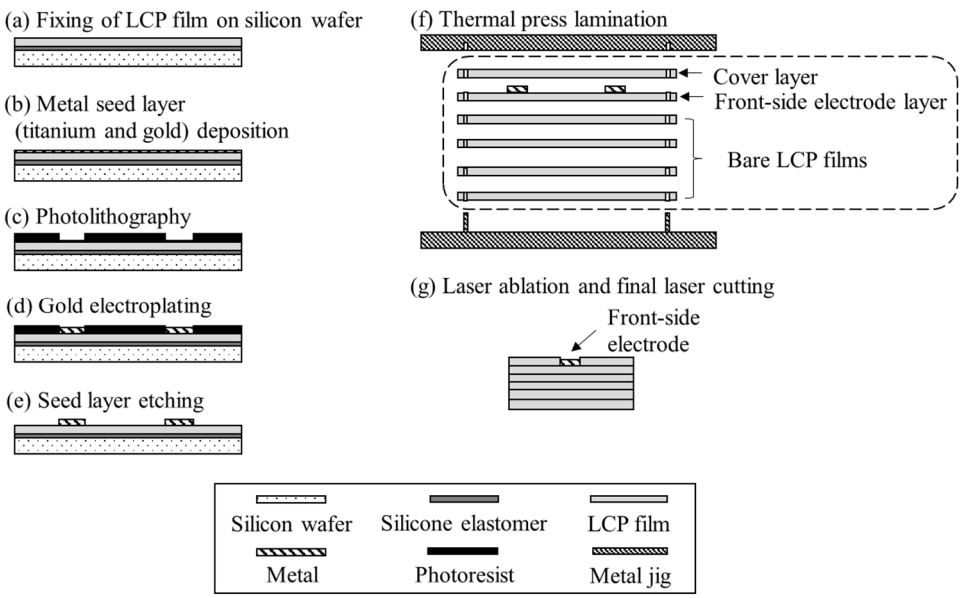

Figure 2.9 Fabrication process of LCP-based single-sided neural probe.

To create the LCP-based tetrode, which has four electrode at the tip of the electrode shank, the same fabrication processes as previously describe is used with a photolithography mask for the tetrode. For the tetrode, four tip electrodes are created in the final laser cutting step. The fabrication process of the LCP-based tetrode is schematically shown in Figure 2.10.

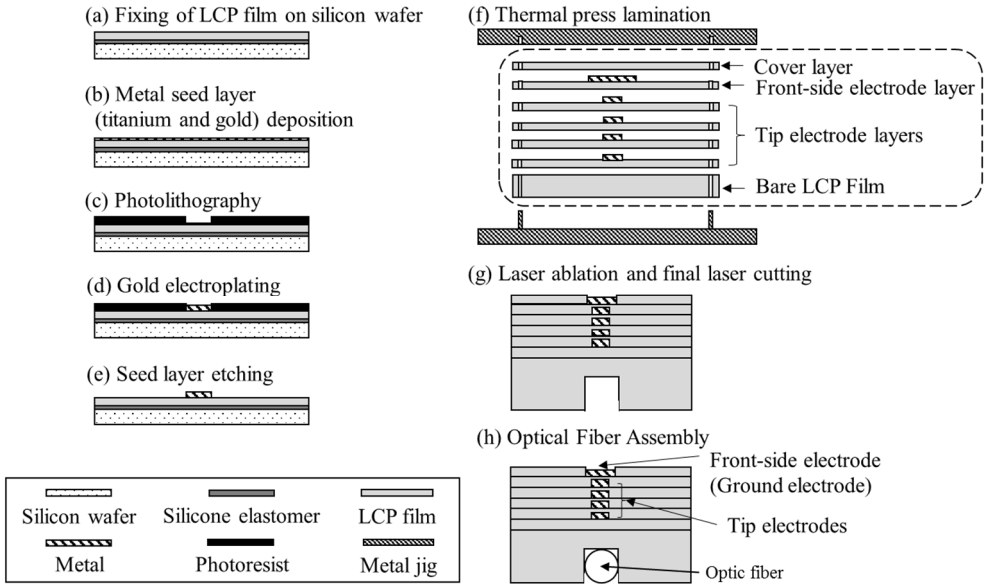

Figure 2.10 Fabrication process of LCP-based tetrode.

The fabrication process of the LCP-based depth-type stimulation electrode is schematically shown in Figure 2.11. To make electrodes on the front and back side and at the tip of the electrode shank, eight metal patterned LCP layers are made through the micro-fabrication processes. In the thermal lamination step, LCP films for one tip electrode and three back-side electrodes are laid on a metal jig upside down, as shown in Figure 2.11 (f). Consequently, the metal patterns of these layers face the floor, which implies that the electrode pads for one tip electrode and three and back-side electrodes are formed on the back side of the neural probe. Laser ablation creates the electrodes on the front and back sides and the final laser cutting step forms tip electrodes. Finally, the iridium oxide is electrodeposited on the gold electrodes of the fabricated depth-type electrode to be used as a stimulation electrode material with a high charge storage capacity and small electrochemical impedance. The process of electrodeposition of iridium oxide will

be described in detail in 2.4.

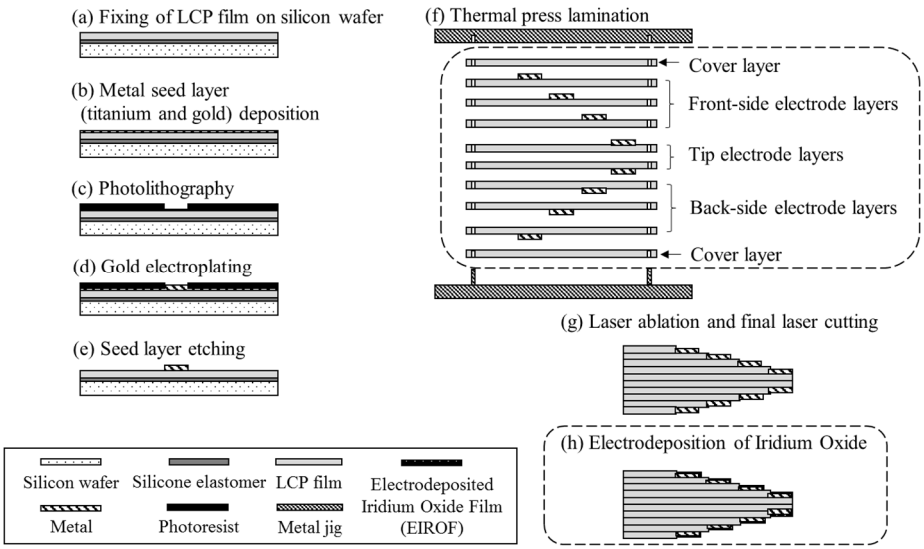

Figure 2.11 Fabrication process of LCP-based depth-type stimulation electrode.

To create the LCP-based optrode, which has four electrode at the tip of the electrode shank and integrated optic fiber, the same fabrication process used for the LCP-based tetrode is used with modified photolithography masks. After the thermal lamination, laser ablation creates a groove for the optic fiber on the back side of the neural probe. And through the final laser cutting, four tip electrodes are made. Finally, the optic fiber is placed in the groove of the fabricated neural probe and the optic fiber is fixed using cyanoacrylate adhesive (Krazy Glue, Borden Inc., Columbus, OH, USA) used as tissue adhesives in other studies [90]-[93]. The optical fiber used is a commercially available multimode optical fiber with ~125 um coating diameter (coating material: polyimide), ~100 um core diameter, and 180-1,150 nm wavelength light (UM22-100, Thorlabs Inc., Newton, NJ, USA). The fabrication process of the LCP-based optrode is schematically shown in Figure

2.12.

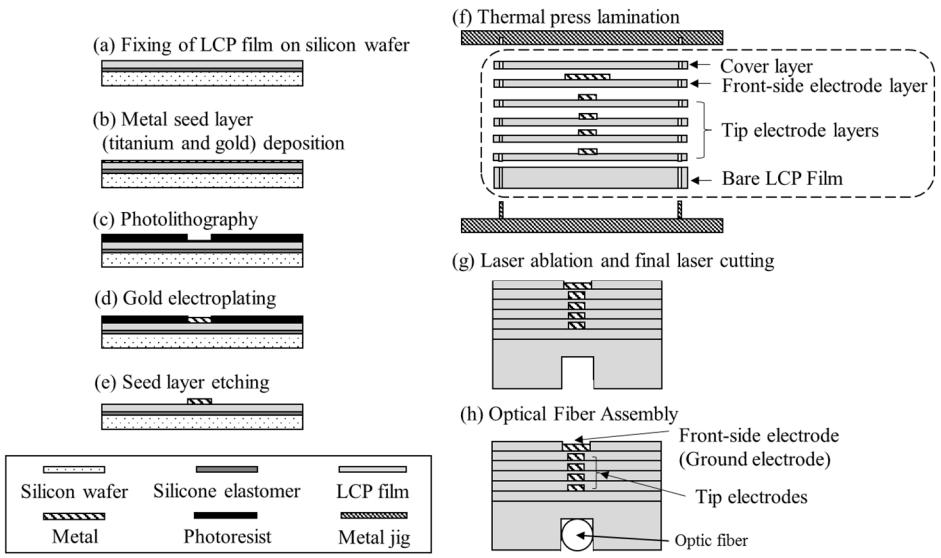

Figure 2.12 Fabrication process of LCP-based optrode.

2.4 Electrochemical Characterization

Electrochemical impedance spectroscopy (EIS) of the fabricated electrodes is characterized using an impedance analyzer (1260 and 1287A, Solartron Analytical, Farnborough, UK) in a phosphate-buffered saline (PBS) solution (Gibco #10010, Invitrogen Life Technologies, Carlsbad, CA, USA) at pH 7.2 with a three-electrode arrangement. The root-mean-square magnitude of the excitation voltage input is 10 mV, and the electrochemical impedance is measured over a frequency range of 1 Hz to 100 kHz.

Additionally, the EIS readings for the fabricated front-side and sidewall electrodes are monitored during *in vitro* accelerated (75 °C) soak tests for 10 days.

The fabricated four-sided neural probes are soaked in a sealed bath filled with a PBS solution maintained at 75 °C in a convection oven. The monitoring of the electrode electrochemical impedance provides information on the electrical connectivity of the interconnection and the status of the metal at the exposed electrode.

2.5 Electrodeposited Iridium Oxide Film (EIROF)

2.5.1 Electrodeposition of Iridium Oxide Film

Iridium oxide is electrodeposited from an aqueous solution of 4 mM $IrCl_4$ in a supporting electrolyte of 40 mM oxalic acid and 340 mM K_2CO_3, similar to the method described in previous studies [55]-[57]. The first step in making the electrodeposition solution is to dissolve the $IrCl_4$ in deionized water; this step took two hours. Into this solution, oxalic acid is dissolved. In another beaker, K_2CO_3 is dissolved in deionized water. The K_2CO_3 solution is then slowly added to the first solution. While mixing the two solutions, the pH is increasing to 10.3. This electrodeposition solution is allowed to sit undisturbed for 48 h before the electrodeposition process. This step allows the establishment of an Ir^{3+}/Ir^{4+} ratio at equilibrium in the solution, which is necessary to obtain stable EIROF films (Figure 2.13).

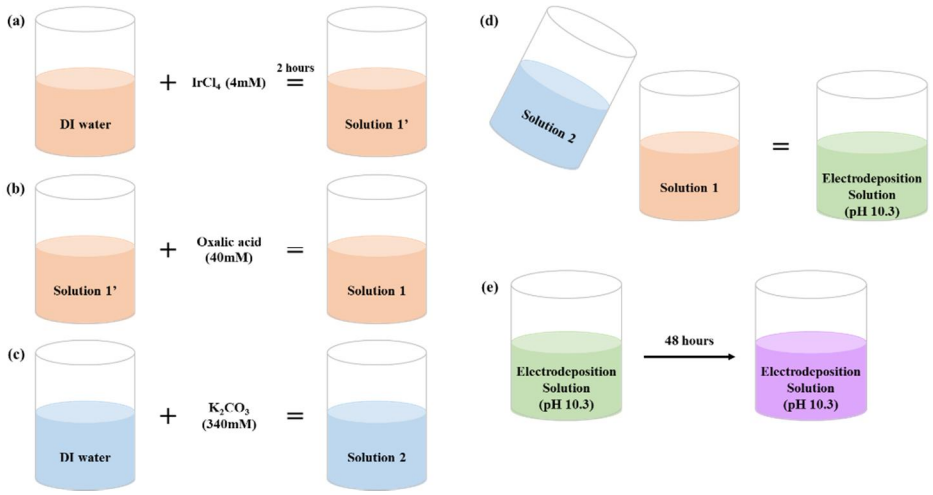

Figure 2.13 Preparation steps of iridium oxide electrodeposition solution.

For the electrodeposition process, a three-electrode system is used consisting of the working electrode (gold electrode site on LCP substrate), a platinum counter electrode, and a silver/silver chloride (3M KCl) reference electrode. The potential is controlled by a potentiostat (Solartron Analytical, 1287A, Farnborough, UK). The potential cycling is a combination of triangular waveforms and rectangular potential pulses. The basic electrodeposition protocol is 50 instances of the triangular waveform between the limits of 0.0 V and 0.55 V versus the Ag/AgCl reference electrode at a 50 mV/s sweep rate followed by 1800 rectangular pulses at 0.55 V (Figure 2.14). The rectangular pulses are applied at 1 Hz with a pulse duration of 0.5 s. After the electrodeposition process, the electrode sites are rinsed with deionized water and dried by N_2 gas. The triangular potential waveforms for the initial stages of the electrodeposition are utilized because they improve EIROF adhesion to substrates. The iridium oxide film is deposited onto the substrate during the potential cycling process, with triangular waveforms

followed by rectangular pulses. To study the effects of the number of repetitions of the triangular waveforms and the rectangular potential pulses, the electrochemical characteristics of iridium oxide films with different numbers of repetitions are made.

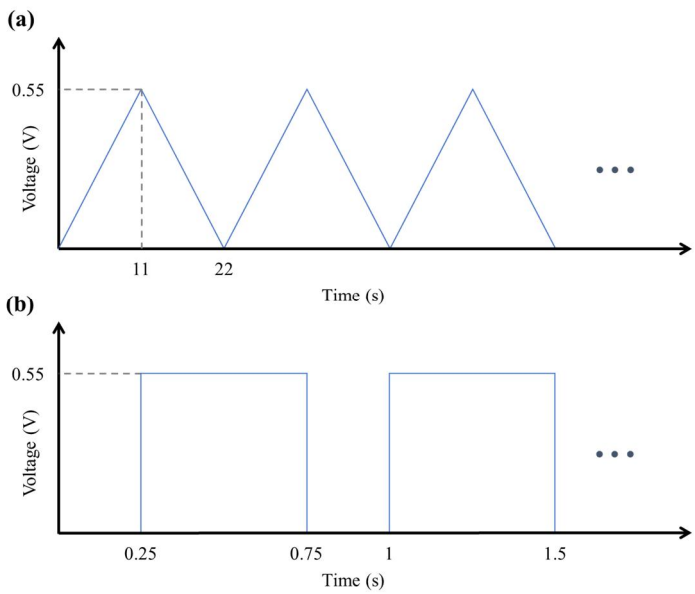

Figure 2.14 Potential cycling for electrodeposition process. (a) Triangular waveforms between limits of 0.0 V and 0.55 V versus the Ag/AgCl reference electrode at a 50 mV/s sweep rate (b) Rectangular pulses at 0.55 V with a pulse rate of 1 Hz and a pulse duration of 0.5 s.

2.5.2 Electrochemical Measurements

The electrochemical impedance of the EIROF electrodes is characterized in a phosphate-buffered saline solution at pH 7.2 using an impedance analyzer in the three-electrode arrangement. The root-mean-square magnitude of the excitation voltage input is 10 mV and the impedance is measured over a frequency range from 1 Hz to 100 kHz. Using the identical electrochemical cell, cyclic voltammetry

is used to measure the cathodic charge storage capacity (CSCc). The electrochemical potential of the electrodes is swept from −0.8 to 0.6 V vs an Ag/AgCl reference electrode at a sweep rate of 100 mV/s. The CSCc value is calculated using the time integral of the cathodic current during the cyclic voltammetry process. Electrochemical measurements are performed before and after the electrodeposition of iridium oxide to compare the electrochemical characteristics of the gold and the iridium oxide. The electrochemical measurements are done with electrodeposited iridium oxide films made with different numbers of repetitions of the triangular waveforms and the rectangular potential pulses.

The charge-injection limit of the fabricated EIROFs is also analyzed. The charge-injection limit is defined as the amount of charge that can be injected through the current stimulus pulse without water decomposition into hydrogen and oxygen. Cathodic current pulses with a pulse width of 1 ms and with varying amplitudes ranging from 0.1 to 1.3 mA are generated using a signal generator (World Precision Instruments, Sarasota, FL, USA). The cathodic current pulses are injected into the EIROF in a phosphate-buffered saline solution. Voltage data are acquired using a digital oscilloscope (Tektronix, DPO 4034, Beaverton, OR, USA) at a sampling rate of 2.5 GS/s.

2.5.3 Surface Morphology and Mechanical Stability

The surface morphology of the EIROF is evaluated by atomic force microscopy (AFM) and scanning electron microscopy (SEM). AFM and SEM

images of a gold electrode before the electrodeposition of iridium oxide are also acquired for comparison of the surface morphologies.

The mechanical stability of the EIROF is tested via a taping test and a sonication test. The taping test is done using a commercial adhesive tape (3M, Scotch Magic Tape 810) applied to a test area of the EIROF. Adhesion is considered adequate if the EIROF surface is not peeled off with the tape when the tape is detached. An ultrasonic wave of 40 kHz is applied at 27 °C for 10 min using an ultrasonic cleaner (Branson Ultrasonic Corporation, Bransonic 3510, Danbury, CT, USA). Impedance measurements and cyclic voltammetry measurements are performed before and after the stability tests to precisely examine the mechanical stability. SEM images and X-ray photoelectron spectroscopy (XPS) are also obtained before and after the stability tests to check the surface morphology and elementary composition.

2.6 *In vivo* Experiments

2.6.1 *In vivo* Neural Signal Recording Experiments

To demonstrate the functionality of the proposed four-sided neural probe and single-sided neural probe, *in vivo* neural signal recording experiments are performed on C57BL/6J (B6) wild-type mice. The mice are deeply anesthetized with 1.5% isoflurane in oxygen, and the skin on the brain and nearby connective tissues are removed. After sterilization, a head plate is implanted on the top of the skull using dental cement. The head is fixed through this head plate, and a small

craniotomy with a diameter of ~1 mm is performed on the top of the primary somatosensory cortex (S1). The LCP-based neural probe is inserted into the S1 position using a precision manipulator. The spontaneous activities are recorded for 10 min after 30 min of stabilization under oxygen inhalation with 1.0 % isoflurane. The signals from the neural probes are amplified at a gain of 515 V/V and a sampling frequency of 20 kHz through an amplifier board (RHD2132, Intan Technologies, Los Angeles, CA, USA) and then filtered at a bandwidth of 0.5–7.5 kHz. All the animals are treated in accordance with the animal research guidelines of the Seoul National University and KAIST.

To analyze the recording data, multi-unit spikes are counted when the peak value (<1 ms) is higher than the threshold, which is set to be four times higher or lower than the median recorded signal measured within a 100-ms window centered around the spike event time.

To evaluate the level of correlation between neural signals recorded from different electrodes in a single probe, a pairwise Pearson correlation coefficient (Pearson's r) analysis and a cross-correlation analysis were performed between the spikes recorded from four electrodes in one shank using MATLAB.

2.6.2 *In vivo* Electrical Stimulation Experiments

To demonstrate the functionality of the proposed depth-type stimulation electrode, *in vivo* stimulation experiments are performed on Sprague-Dawley rats (SD rat) (male, ~ 300g). The rats are anesthetized with an intraperitoneal injection of a 2 mL/kg cocktail of 10 mL of ketamine hydrochloride (50 mg/mL), 1.1 mL of

xylazine hydrochloride (23.32 mg/mL), and 2.67 mL of saline. After anesthetization, rats are fixed on a stereotaxic frame (Narishige, Tokyo, Japan). Their scalps are carefully opened and a small burr hole is made on the target area, medial forebrain bundle (MFB, AP 2.3 mm and ML 1.8 mm from bregma, and DV 8.6 mm from the skull). The fabricated LCP-based depth-type stimulation electrode is inserted into the MFB. This study is conducted according to the guidelines of the Institution Animal Care and Use Committees of Yonsei University and Seoul National University.

MFB is known as a part of the reward system, involved in the integration of reward and pleasure [94]. Therefore, electrical stimulation of the MFB can be used as a cue stimulus to control animal behavior [95], [96]. After implantation, Intra Cranial Self–Stimulation (ICSS) is conducted in the MFB to develop operant condition. ICSS tests begin 3 days after surgery in the Skinner Box. A lever press delivers a stimulation train to the MFB (burst with : 500 ms, pulse duration: 0.2-0.5 ms, pulse rate : 30-50 Hz, pulse amplitude: 0.15–0.20 mA) (Figure 2.15)

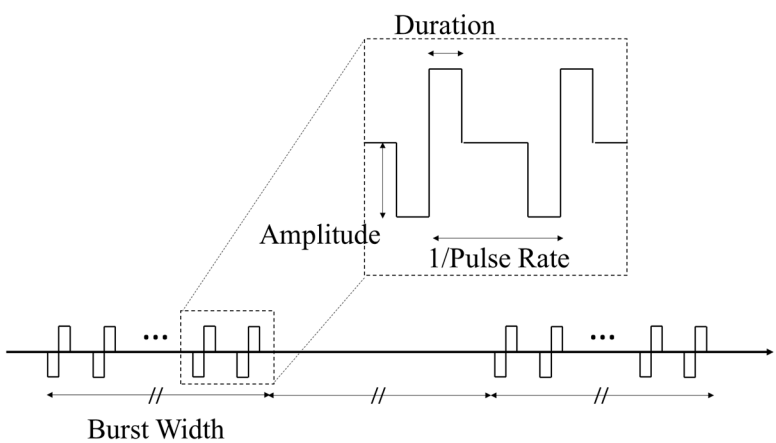

Figure 2.15 Biphasic electrical stimulation waveform.

To verify the performance of the proposed EIROF as an electrode material, *in vivo* experiments are done. The electrical stimulation and recording are done simultaneously using a LCP-based neural electrode. The LCP-based neural electrode has four channels; one of these is used for electrical stimulation and the others are used as recording electrodes. For the experiments, SD rats (male, 170–190g, n=15) with a neuropathic pain model are used. In order to induce neuropathic pain in the rats, surgical procedures are used as described in the previous studies [39], [78], [97], [98]. This study is conducted according to the guidelines of the ethics committee of the International Association for the Study of Pain [99] and the Institution Animal Care and Use Committees of Yonsei University and Seoul National University.

After neuropathic pain is induced, electrical stimulation is performed while the local field potential (LFP) is monitored from the ventral posterolateral nucleus (VPL, AP 2.2 mm and ML 2.8 mm from bregma, and DV 6.0 mm from the skull [100]) to suppress neuropathic pain and monitor how the electrical stimulation alters the activity from the neighboring neurons. For the surgical procedures, the rats are anesthetized with pentobarbital sodium (50 mg/kg) and are fixed on a stereotaxic frame. Their scalps are carefully opened and a small burr hole is made on the target area (VPL). The fabricated LCP-based EIROF microelectrode is inserted into the VPL. The electrode is firmly fixed on the skull, and the scalp is closed with sutures for permanent fixation of the electrode. One week later with

animal care, the rats are anesthetized with urethane (1.3 g/kg) for the LFP recordings. The electrodes are connected to an acquisition system consisting of a differential amplifier (Model 1700; A-M Systems, Sequim, WA, USA) and an AD converter (Micro 1401; Cambridge Electronic Design Limited, Cambridge, United Kingdom). Acquired signals are stored and displayed in a multi-channel continuous data acquisition and analysis package (Spike2, version 7, Cambridge Electronic Design Limited, Cambridge, UK).

To invoke pain by cold stimulus (cold allodynia), 0.1 mL of acetone is dropped onto the rat's contralateral hind paw. The detailed procedures for evoking cold allodynia and electrophysiological monitoring are presented in the previous report [39]. Neuronal activity changes due to the electrical stimulation of the VPL are monitored simultaneously. Cathodic-first (biphasic) current pulses with an amplitude of 1.4 mA, a pulse rate of 130 Hz, and a pulse duration of 60 μs are delivered to the VPL.

2.6.3 *In vivo* Optical Stimulation and Electrical Recording Experiments

To demonstrate the functionality of the proposed LCP-based tetrode and optrode, *in vivo* neural signal recording experiments are performed on CaMKIIa-ChR2-EYFP mice with optical stimulation. The mice are deeply anesthetized with 1.5% isoflurane in oxygen, and the skin on the brain and nearby connective tissues are removed. After sterilization, a head plate is implanted on the top of the skull using dental cement. The head is fixed through this head plate, and a small craniotomy with a diameter of ~1 mm is performed on the top of the target area

(primary visual cortex (V1), posterior parietal cortex, and hippocampus). The fabricated neural probe is inserted into the target area using a precision manipulator. The spontaneous activities and light-evoked activities are recorded for 3 min after 30 min of stabilization under oxygen inhalation with 1.0 % isoflurane. The signals from the neural probes are amplified at a gain of 515 V/V and a sampling frequency of 20 kHz through an amplifier board (RHD2132, Intan Technologies, Los Angeles, CA, USA) and then filtered at a bandwidth of 0.5–7.5 kHz. All the animals are treated in accordance with the animal research guidelines of the Seoul National University and KAIST.

A blue laser (473 nm, Shanghai Laser & Optics Century Co., Shanghai, China) of power 1-1.5 mW is used for light stimulation. Light stimulation is delivered to the target area through an optic fiber. The optic fiber is located upon the target area for the LCP-based tetrode experiment, on the outside of the experimental animal. In the case of the LCP-based optrode experiment, the optic fiber is inserted into the target area where the neural probe is located because the fiber is integrated to the probe. The light stimulation is on for 1 sec and off before and after the light stimulation for 2 sec each. The 5 sec light stimulation on/off block is repeated during the recording period (3 min) (Figure 2.16).

To analyze the recording data, multi-unit spikes are counted when the peak value (<1 ms) is higher than the threshold, which is set to be six times higher or lower than the median recorded signal measured within a 100-ms window centered around the spike event time.

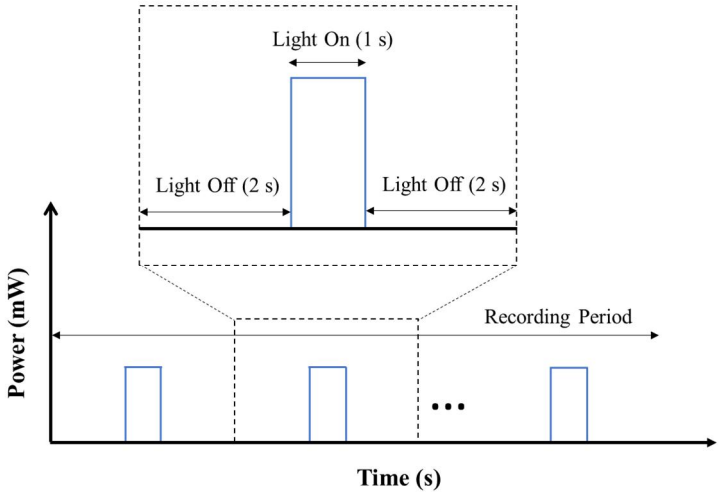

Figure 2.16 Light stimulation cycle.

Chapter III

Results

3.1 Neural Probes

3.1.1 Recording Probes

3.1.1.1 Four-sided Neural Probe

The fabricated LCP-based four-sided neural probe and scanning electron microscope (SEM) images of the electrodes are shown in Figure 3.1. A laser ablation process opens a 40 μm × 40 μm area on the front and back of the electrode shank, respectively. The sidewall electrodes were formed by the laser cutting process. The exposed area of the sidewall electrodes was 4–5 μm (thickness of the electroplated metal) × 100 μm. Figure 3.1 (b) shows a SEM image of the probe tip to depict the quality of laser micromachining.

3.1.1.2 Single-sided Neural Probe

Figure 3.2 shows the fabricated LCP-based single-sided neural probe. The electrodes of the single-sided neural probe were formed by the laser ablation process. The size of the electrodes is 40 μm × 40 μm.

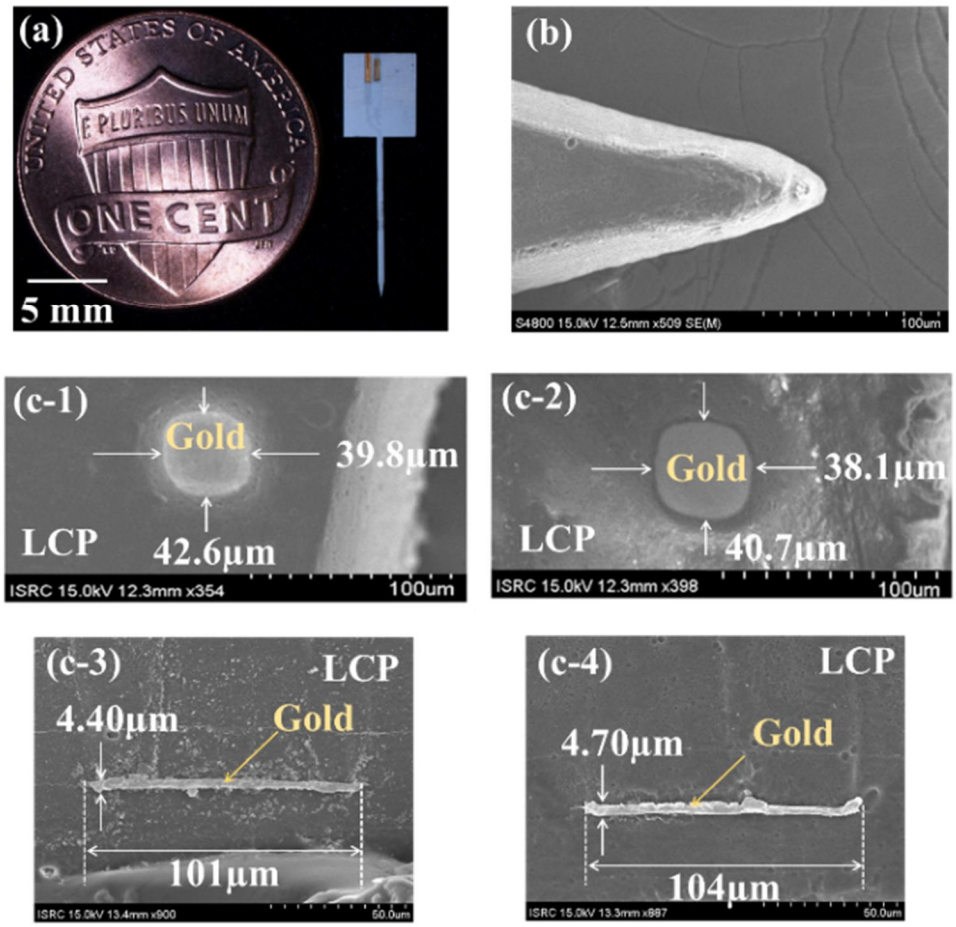

Figure 3.1 (a) Fabricated LCP-based neural probe with four-sided electrodes. (b) Scanning electron microscope (SEM) image of the probe tip. SEM images of electrodes: (c-1) front-side electrode (the white strip on the right shows the partial view of the left-side of the probe.), (c-2) back-side electrode, (c-3) left-sidewall electrode, and (c-4) right-sidewall electrode.

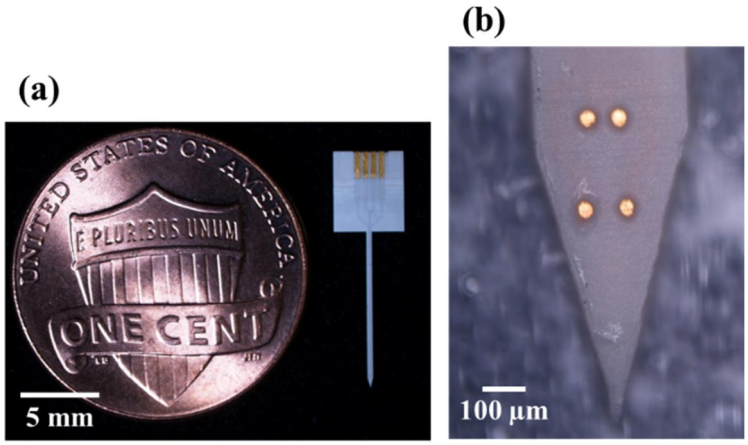

Figure 3.2 (a) Fabricated LCP-based neural probe with single-sided electrodes. (b) Microscopic images of the fabricated single-sided neural probe.

3.1.1.3 Tetrode

Figure 3.3 shows the fabricated LCP-based tetrode. The LCP-based tetrode has four electrodes with size of 10 µm (thickness of the electroplated metal) × 100 µm located at the tip of the electrode shank.

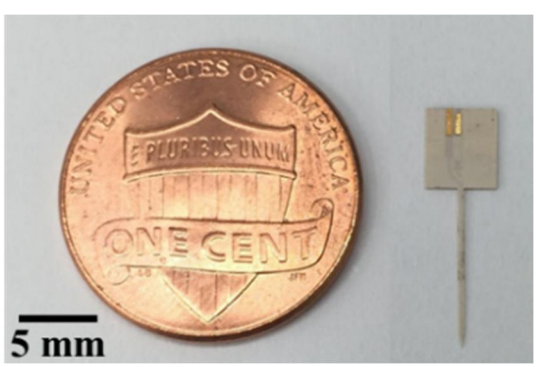

Figure 3.3 Fabricated LCP-based tetrode.

3.1.2 Depth-type Stimulation Electrode

Figure 3.4 shows the fabricated depth-type stimulation electrode. Three

electrodes with size of 20 μm × 75 μm are located on the front and another three electrodes on the back side of the electrode shank. And two electrodes with size of 10 μm (thickness of the electroplated metal) × 150 μm formed at the tip of the electrode shank. All of the electrodes are electrodeposited with iridium oxide.

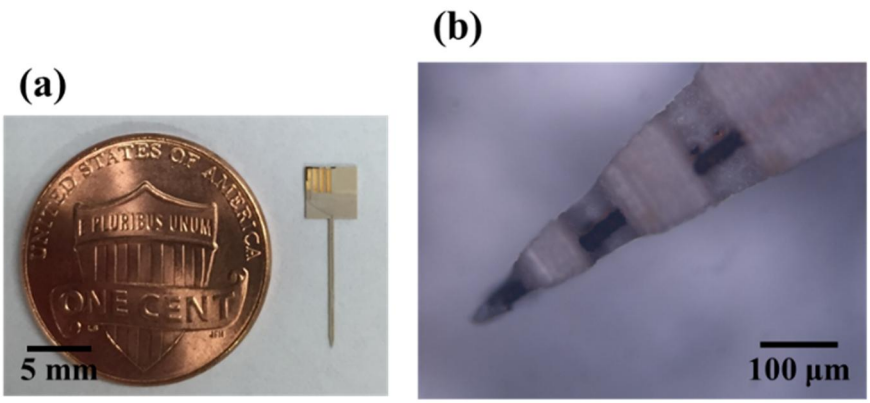

Figure 3.4 (a) Fabricated LCP-based depth-type stimulation electrode. (b) Microscopic images of the fabricated depth-type stimulation electrode.

3.1.3 Optrode

Figure 3.5 shows the fabricated LCP-based optrode with four tip electrodes. The size of the electrodes is 10 μm (thickness of the electroplated metal) × 100 μm. The optic fiber is fixed to the neural probe

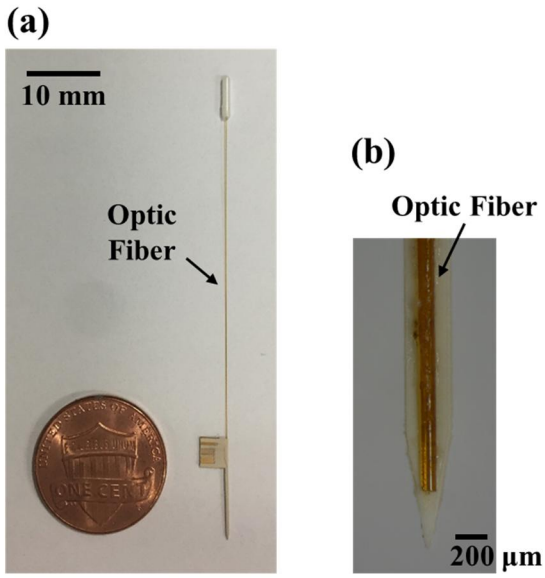

Figure 3.5 Fabricated LCP-based optrode.

3.2 Electrochemical Characterization

The EIS results for the four-sided neural probe are shown in Figure 3.6. The electrochemical impedance of the front- and back-side electrodes was 302.44 ± 117.88 kΩ at 1 kHz (gold), and that of the electrodes located on the sidewall was 140.67 ± 57.74 kΩ (gold). The EIS results for the single-sided neural probe are also shown in Figure 3.6. The electrochemical impedance of the front-side electrodes was 342.40 ± 185.19 kΩ at 1 kHz (gold). The electrochemical impedance of tip electrodes of the LCP-based tetrode 299.6 ± 129.78 kΩ at 1 kHz (gold). The electrochemical impedance of the front- and back-side electrodes of the LCP-based depth-type stimulation electrode 4.23 ± 2.10 kΩ at 1 kHz (Electrodeposited iridium oxide film, EIROF). And the electrochemical impedance of the tip electrodes of the LCP-based depth-type stimulation electrode 4.78 ± 2.34 kΩ at 1 kHz (EIROF). The

electrochemical impedance of tip electrodes of the LCP-based optrode 173.04 ± 61.71 kΩ at 1 kHz (gold).

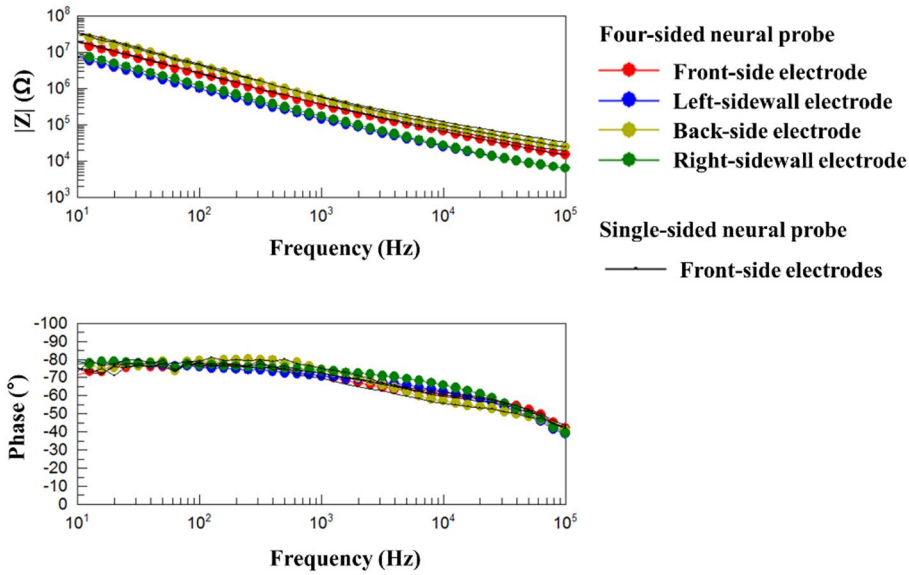

Figure 3.6 Electrochemical impedance spectroscopy (EIS) of the fabricated LCP-based neural probes with four-sided electrodes and single-sided electrodes.

The electrode electrochemical impedance levels of the fabricated front-side and sidewall electrodes are monitored during an *in vitro* accelerated soak test at 75 °C. The electrochemical impedance is measured after 1 hour and on day 1, day 2, day 5, and day 10 after soaking the neural probe in a PBS solution. As shown in Figure 3.7, the EIS results for the front-side and sidewall electrodes remains the same for 10 days. These results indicated that the electrical interconnections of both the front-side and sidewall electrodes are sustained, which implied that the exposed electrodes on the front side and sidewall are well preserved during the test period.

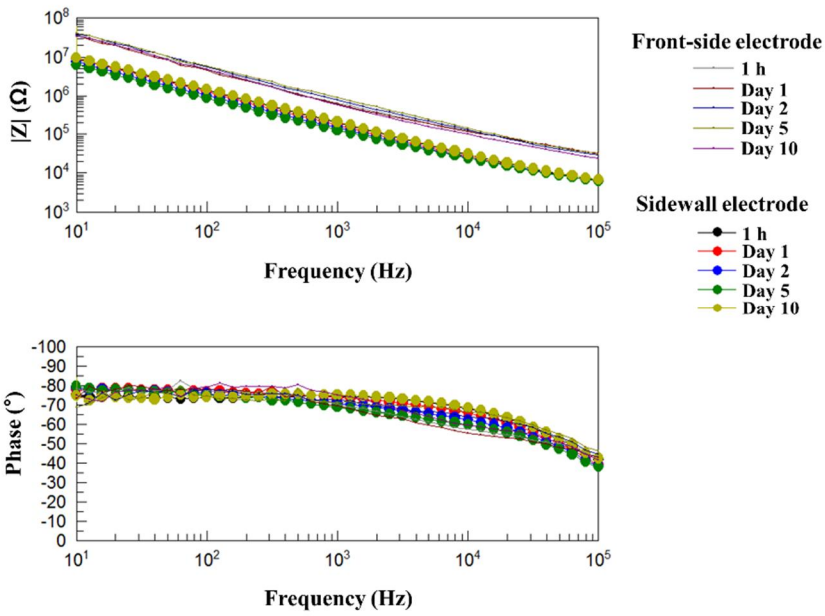

Figure 3.7 Soak test (10days, 75 °C) results and EIS results for the front-side and sidewall electrodes.

3.3 Electrodeposited Iridium Oxide Film

3.3.1 Electrochemical Measurements

Figure 3.8 shows the LCP-based gold microelectrode before the electrodeposition of the iridium oxide and the electrodeposited iridium oxide film on the LCP-based microelectrode (diameter of the electrode sites: 300 μm). The EIROF is formed on the gold electrodes by potentiodynamic deposition using triangular potential waveforms followed by rectangular pulses. The cathodic charge storage capacity (CSC_C) and the electrochemical impedance at 1 kHz are measured before and after the electroplating of the iridium oxide onto the gold layer. The

cyclic voltammetry (CV) curves and the electrochemical impedance spectroscopy (EIS) results are shown in Figure 3.9. The CSC_C values are calculated from the CV curves, as explained in the methods section. Before the electrodeposition of the iridium oxide, the electrochemical impedance of the gold electrode sites at 1 kHz and the cathodic charge storage capacity are measured and found to be 26.65 ± 6.93 kΩ and 0.32 ± 0.05 mC/cm^2, respectively. Likewise, values of 1.41 ± 1.1 kΩ and 24.19 ± 6.21 mC/cm^2 are measured after the electrodeposition of the iridium oxide. The cathodic charge storage capacity is increased and the electrochemical impedance at 1 kHz is decreased after the iridium oxide electroplating process, as expected.

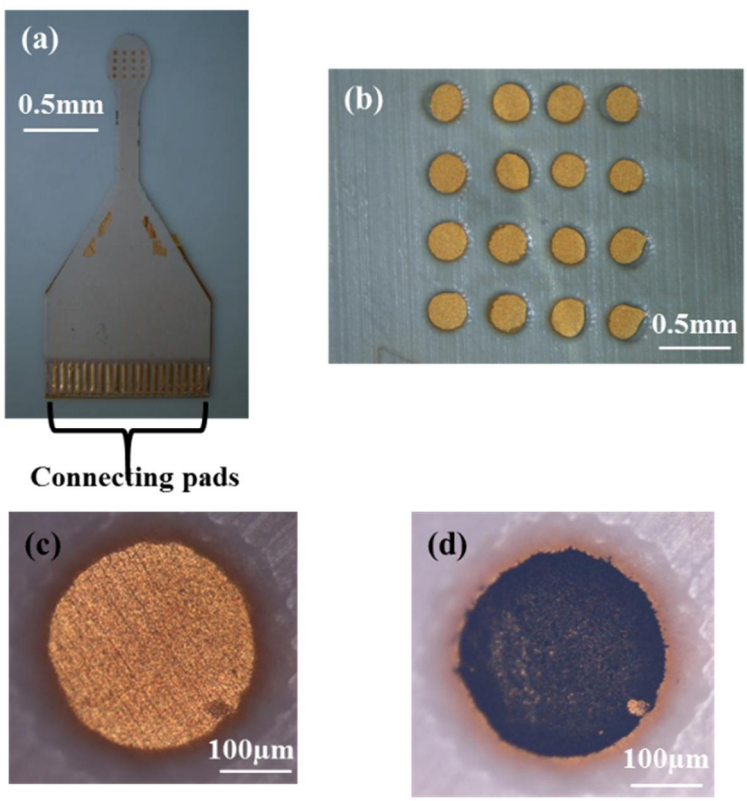

Figure 3.8 (a), (b) LCP-based microelectrodes with gold electrode sites before the electrodeposition of iridium oxide. (c) Gold electrode site and (b) electrodeposited iridium oxide film (EIROF) electrode site (diameter of the electrode sites: 300 μm).

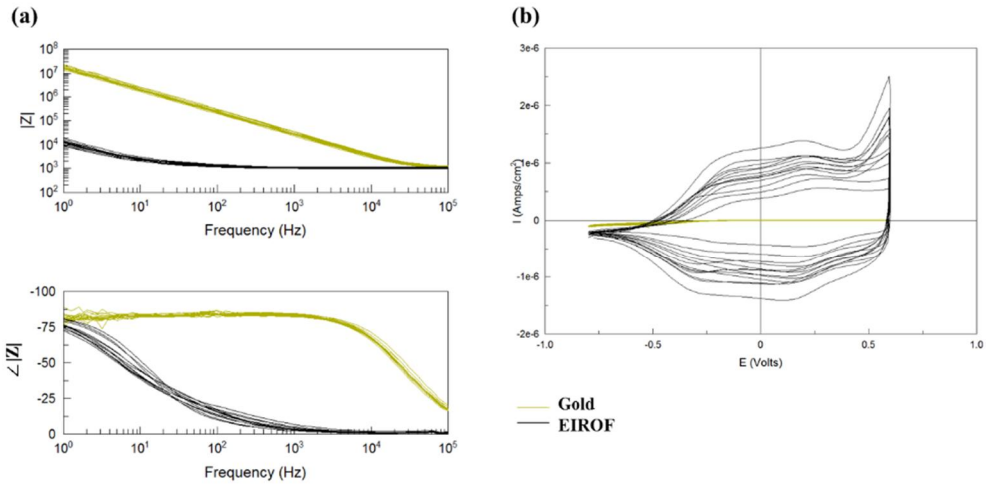

Figure 3.9 (a) Electrochemical impedance results of gold and EIROFs and (b) cyclic volammetry (CV) curves of the gold and EIROFs.

To examine the effects of the number of repetitions of the rectangular potential pulse, the rectangular pulses are applied 1800, 3600, and 5400 times. The cathodic charge storage capacity is increased as the number of rectangular pulses increased, as shown in Table 3.1 and Figure 3.10. However, the electrochemical impedance is nearly identical, indicating that an increase in the number of rectangular potential pulses leads to a higher charge storage capacity in the EIROF.

Table 3.1 Results showing the electrochemical characteristics with different numbers of repetitions of rectangular potential pulses (number of triangular waveforms: 50).

Number of rectangular pulses	Electrochemical impedance at 1 kHz (kΩ)	Cathodic charge storage capacity (CSC_C) (mC/cm^2)
1800	1.44	11.13
3600	1.13	20.24
5400	1.10	25.58

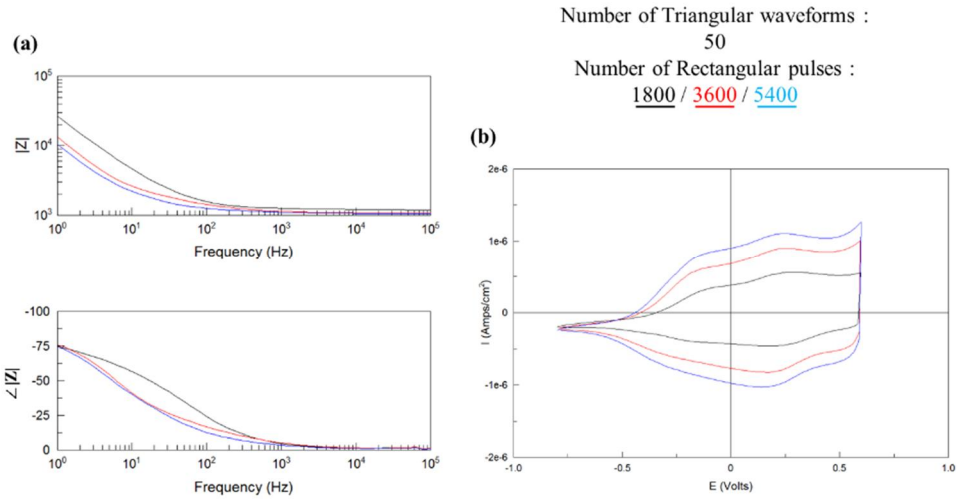

Figure 3.10 Results showing the electrochemical characteristics of EIROFs formed using fifty triangular waveforms and different numbers of rectangular potential pulses. (a) Electrochemical impedance results of gold and EIROFs and (b) CV curves of gold and EIROFs [numbers of rectangular pulses: 1800 (black), 3600 (red), and 5400 (blue)].

However, the cathodic charge storage capacity and electrochemical

impedance of EIROFs made with different numbers of repetitions of the triangular waveforms (50, 100, 200, and 400 times) do not show a constant increasing or decreasing trend, as shown in Table 3.2 and Figure 3.11. Because the triangular waveforms are known to affect the surface adhesion strength [55], the mechanical stability levels of EIROFs formed with different numbers of triangular waveforms are measured as described in the following section.

Table 3.2 Results showing the electrochemical characteristics for different numbers of repetitions of triangular waveforms (number of rectangular pulses: 3600).

Number of triangular waveforms	Electrochemical impedance at 1 kHz (kΩ)	Cathodic charge storage capacity (CSC_C) (mC/cm^2)
50	1.13	20.24
100	1.09	22.89
200	1.00	25.97
400	1.15	24.26

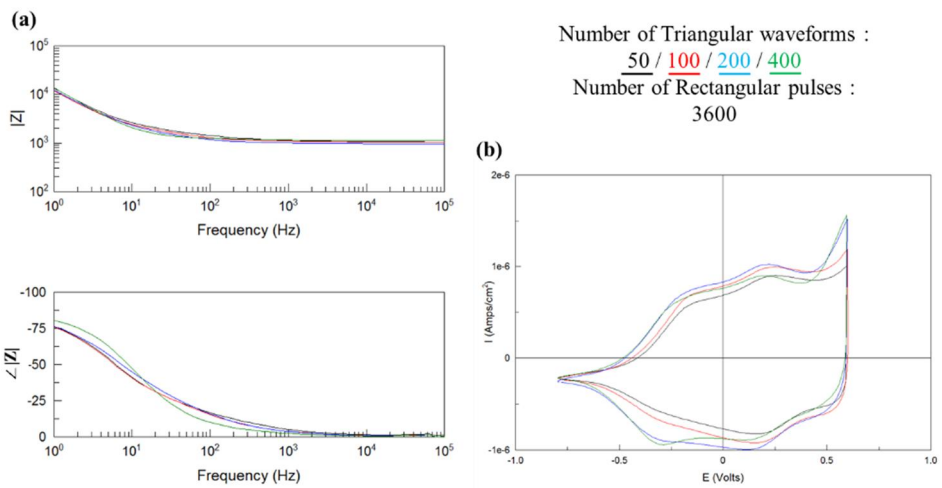

Figure 3.11 Results showing the electrochemical characteristics of EIROFs formed using different numbers of triangular waveforms and 1800 rectangular potential

pulses. (a) Electrochemical impedance results of gold and EIROFs and (b) CV curves of gold and EIROFs [numbers of triangular waveforms: 50 (black), 100 (red), 200 (blue), and 400 (green)].

Figure 3.12 (a) shows the 1 ms cathodal current pulses ranging from 0.1–1.3 mA used for charge-injection limit analysis. During the current pulses flowing through the EIROF electrodes in PBS, the induced voltage transients are recorded and plotted in Figure 3.12 (b). Taking the lower voltage limit of the water window (−0.645 V vs the Ag/AgCl reference electrode), the charge-injection limit of the fabricated EIROF is determined to be 1.27 mC/cm^2. The charge storage capacity of the EIROF used for the charge-injection limit analysis was 23.54 mC/cm^2.

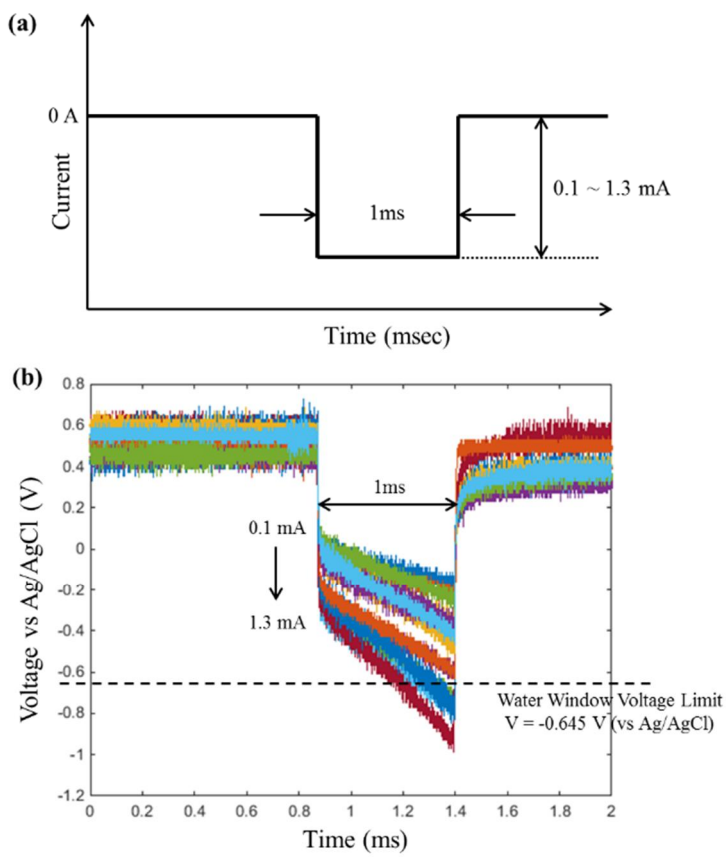

Figure 3.12 (a) Current pulse used for the charge-injection limit analysis (b) Voltage responses from the charge-injection limit analysis recorded from the EIROFs.

3.3.2 Surface Morphology and Mechanical Stability

In general, the effective surface of an electrode is proportional to the roughness of the electrode surface. When the roughness and porosity increase, the actual surface for an active chemical reaction between the electrode and the electrolyte also increases. In order to characterize the morphology of electrode surfaces, AFM and SEM images of the gold and EIROF are obtained and depicted in Figure 3.13 and Figure 3.14, respectively. As shown in these images, the EIROF clearly has a rougher surface than gold, which facilitates effective neural stimulation with a large active surface area.

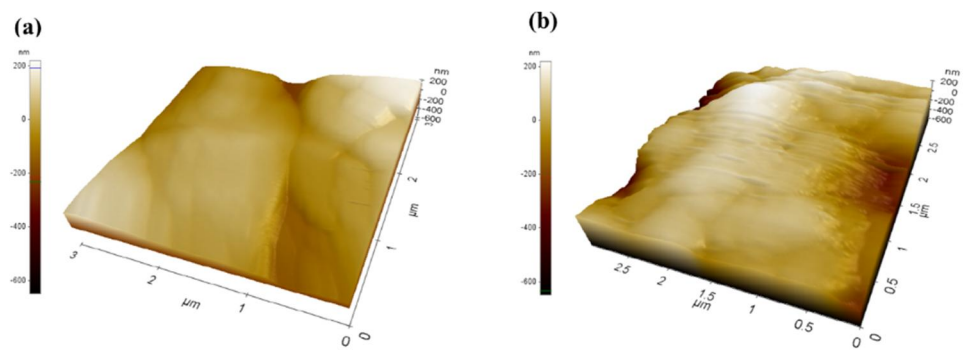

Figure 3.13 Atomic force microscopy (AFM) images of (a) gold and (b) EIROF formed using 50 triangular waveforms and 5400 rectangular potential pulses.

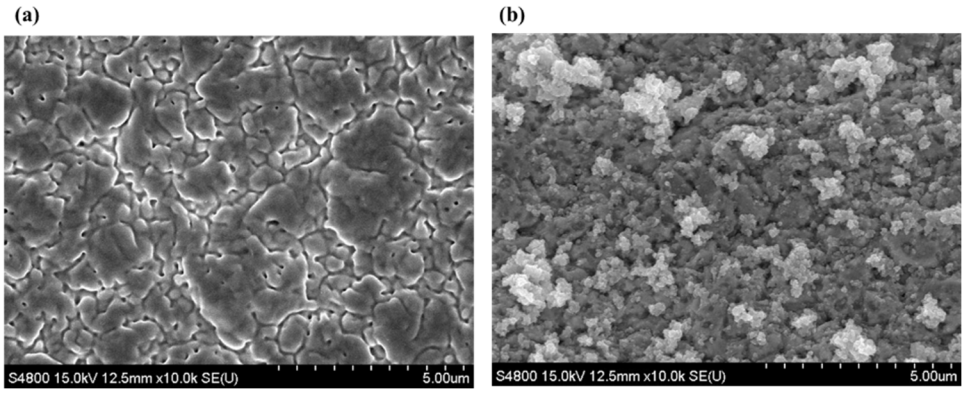

Figure 3.14 SEM images of (a) gold and (b) EIROF formed using 50 triangular waveforms and 3600 rectangular potential pulses.

Mechanical stability of neural electrodes is required for implantable stimulating electrodes. To test the mechanical stability of the fabricated EIROF, a taping test and a sonication test are conducted. Taping tests are performed three times with tapes attached to the EIROF surfaces. The tape is placed on the surface of the substrate covering the electrode sites and then removed quickly by hand. Failures can occur at the weakest points of the electrode, such as the junction between the EIROF and LCP film. In the taping tests, however, no detachments between the EIROF and LCP interface are observed and the electrochemical characteristics were maintained (Figure 3.15).

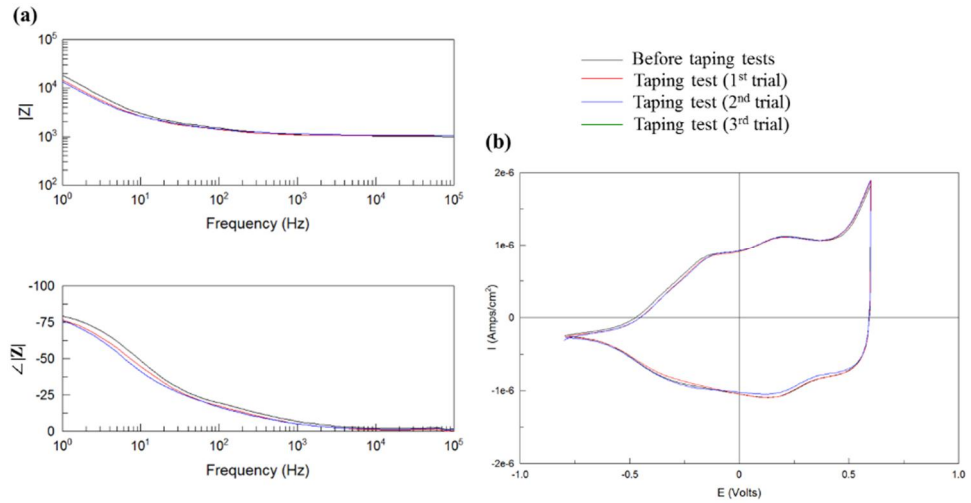

Figure 3.15 Results showing the electrochemical characteristics before and after the taping tests. The EIROF is made with 50 triangular waveforms and 5400 rectangular potential pulses. (a) Electrochemical impedance results and (b) cyclic voltammetry curves [black: before the taping tests, red: taping test (first trial), blue: taping test (second trial), green: taping test (third trial)].

A triangular waveform in electrodeposition is known to improve EIROF adhesion to a substrate [55]. Accordingly, in order to investigate the effects of the triangular waveform, the EIROFs are deposited with different repetitions of the triangular waveform ranging from 50 to 400, and another stability test is performed, a sonication test, using an ultrasonic cleaner. Figure 3.16 and Table 3.3 show the electrochemical impedance at 1 kHz and the cathodic charge storage capacity before and after the sonication tests. As shown in the results, the electrochemical impedance is increased and the CSCc value is decreased after the sonication tests. In Figure 3.17, scanning electron microscope (SEM) images of EIROFs formed with different numbers of triangular waveforms before and after the sonication tests

are shown. The white matter in this figure, presumably iridium particles, seems to disappear significantly after the sonication tests regardless of the number of applied triangular waves. To study the effects of the applied triangular waveforms quantitatively, the surfaces of EIROFs are analyzed using XPS measurements (Figure 3.18). According to the XPS results, the atomic percentages of the iridium in EIROFs made with 50 triangular waveforms decrease by 2.9%, while the EIROFs created with 400 triangular waveforms shows a 1.6% decrease. Based on these results, the number of applied triangular waveforms affects the mechanical stability of the EIROFs.

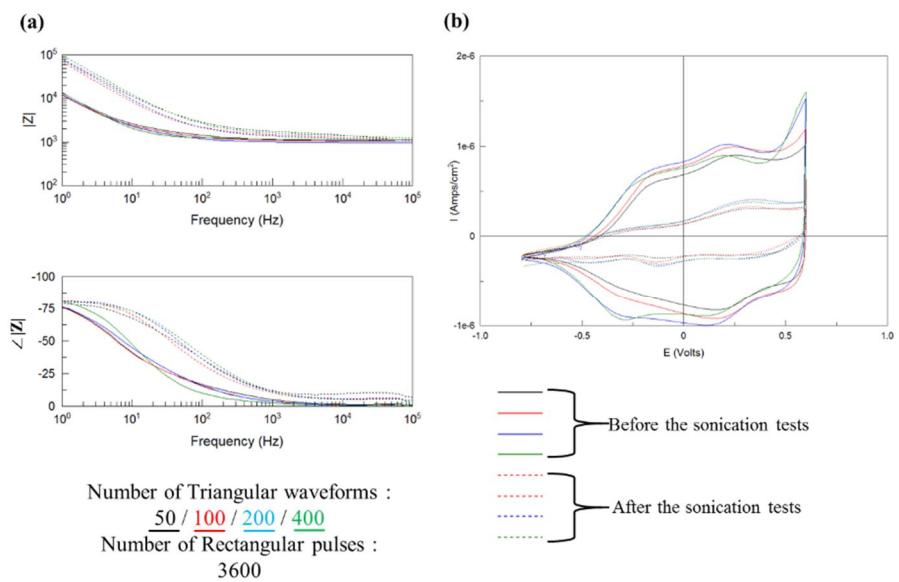

Figure 3.16 Results showing the electrochemical characteristics before and after the sonication tests. The EIROFs are made with different numbers of triangular waveforms and with 3600 rectangular potential pulses. (a) Electrochemical impedance results and (b) cyclic voltammetry curves [numbers of triangular waveforms: 50 (black), 100 (red), 200 (blue), and 400 (green)] (straight lines: before the sonication tests, dotted lines: after the sonication tests).

Table 3.3 Results showing the electrochemical characteristics for different numbers of repetitions of triangular waveforms before and after the sonication tests (number of rectangular pulses: 3600).

Number of triangular waveforms	Electrochemical impedance at 1 kHz (kΩ)		Cathodic charge storage capacity (CSC_C) (mC/cm^2)	
	Before the sonication tests	After the sonication tests	Before the sonication tests	After the sonication tests
50	1.13	1.75	20.24	6.68
100	1.09	1.45	22.89	6.88
200	1.00	1.38	25.97	7.86
400	1.15	1.59	24.26	8.36

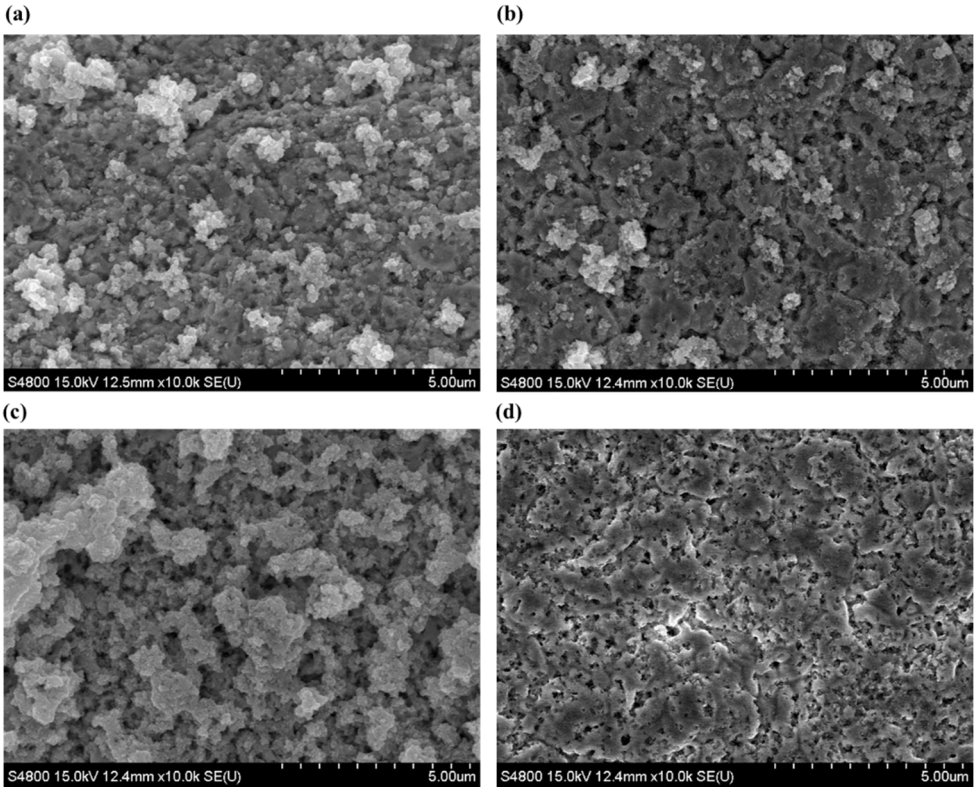

Figure 3.17 SEM images of EIROFs: (a) and (b) are EIROFs made with 50 triangular waveforms and 3600 rectangular potential pulses, and (c) and (d) are EIROFs formed with 400 triangular waveforms and 3600 rectangular potential pulses. (a) and (c) are EIROFs before the sonication tests, and (b) and (d) are EIROFs after the sonication tests.

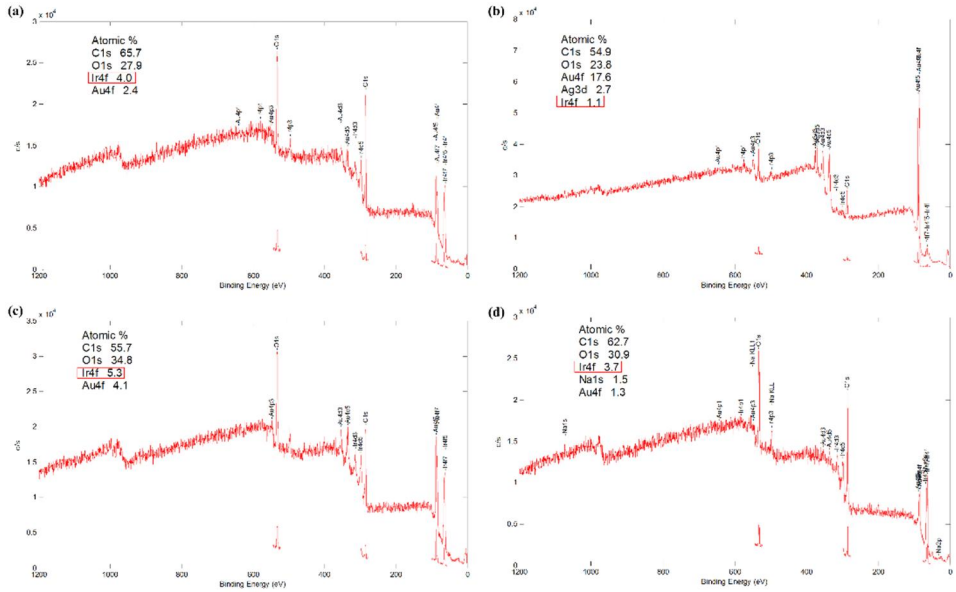

Figure 3.18 X-ray photoelectron spectroscopy (XPS) measurement results: (a) and (b) are EIROFs made with 50 triangular waveforms and 3600 rectangular potential pulses, and (c) and (d) are EIROFs formed with 400 triangular waveforms and 3600 rectangular potential pulses. (a) and (c) are EIROFs before the sonication tests, and (b) and (d) are EIROFs after the sonication tests.

3.4 *In vivo* Experiments

3.4.1 *In vivo* Neural Signal Recording Experiments

The results of *in vivo* neural signal recording for the four-sided and single-sided neural probes are shown in Figure 3.19 and Figure 3.20, respectively. For the four-sided neural probe, the patterns of spikes recorded from the four channels are significantly different from each other. On the other hand, for the single-sided probe, the four channels mostly collects identical spike patterns. As shown in Figure 3.20, the single-sided neural probe collects more identical spikes patterns than the four-sided neural probe (Figure 3.19).

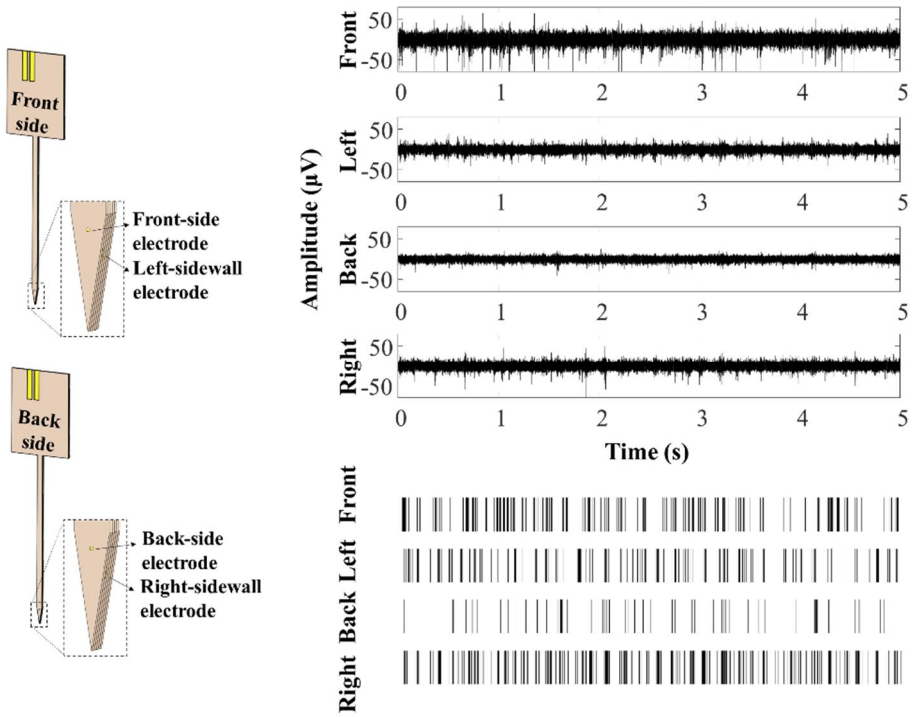

Figure 3.19 Experimental results of *in vivo* neural signal recording for the four-sided neural probe: raw traces and the raster plot.

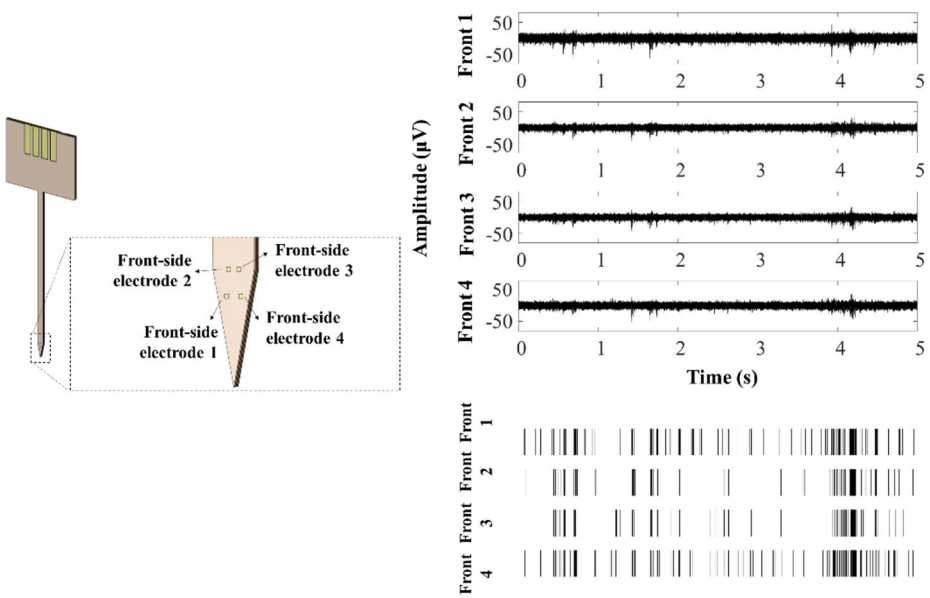

Figure 3.20 *In vivo* neural signal recording experimental results of the single-sided neural probe: raw traces and raster plot.

To analyze the correlation between the neural signals recorded by different recording electrodes of one neural probe, a pairwise Pearson correlation coefficient (Pearson's r) analysis (Figure 3.21 (a)) and a cross-correlation analysis (Figure 3.21 (b)) are carried out on signals from different channels of either the four-sided neural probe or the single-sided neural probe. Both high r values and high cross-correlation coefficient values at time 0 indicate a more positive correlation between the neural activities recorded from different channels. As listed in Table 3.4 and shown in Figure 3.21, whereas the four front-side electrodes of the single-sided neural probe records highly correlated neural signals, the four electrodes of the four-sided neural probe records neural signals that showed only a weak correlation. The distances for the four-sided neural probe are 1.36-4.9 times greater than those for the single-sided neural probe; however, the Pearson correlation coefficients for the single-sided neural probe are more than 10 times greater than those for the four-sided neural probe. These results support the contention that the four-sided neural probe can record a greater variety of *in vivo* neural activities simultaneously than the single-sided probe.

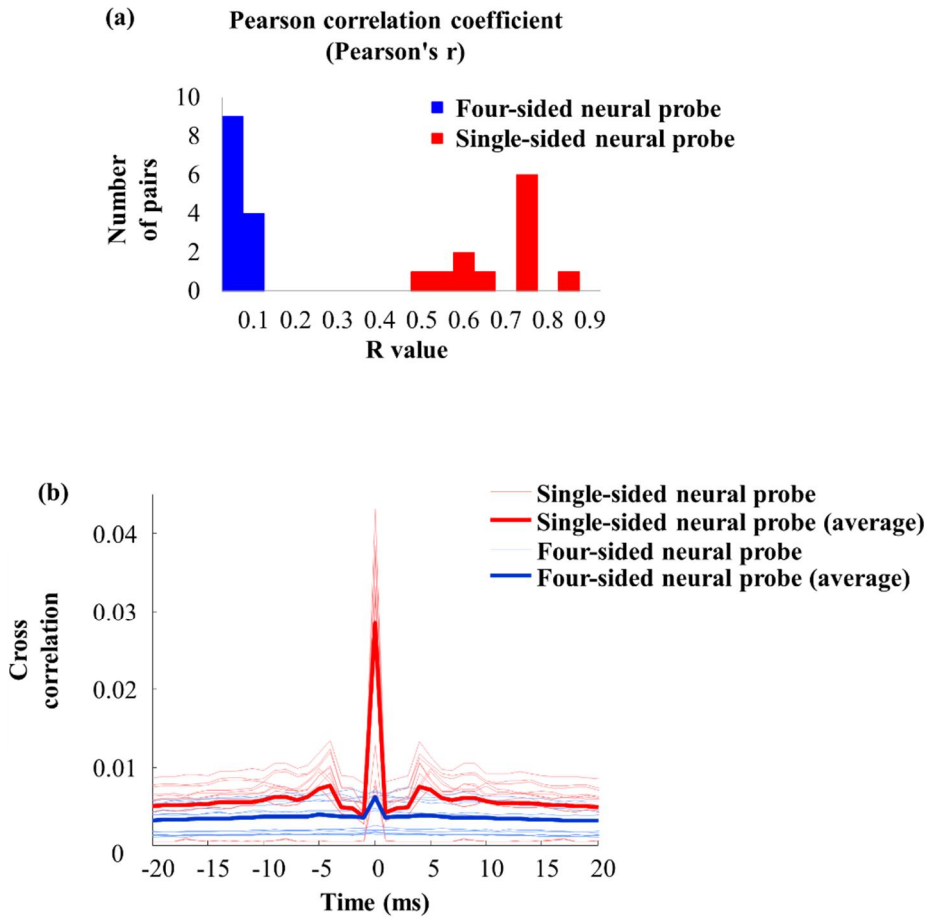

Figure 3.21 (a) Pearson correlation coefficient (Pearson's r) analysis results and (b) cross-correlation analysis results of the recorded *in vivo* neural signals for the four-sided and single-sided neural probes.

Table 3.4 Distances and Pearson's correlation coefficient (Pearson's r value) between all recording electrode pairs of the four-sided and single-sided neural probes.

Four-sided neural probe							
Recording electrode pair		Front ↔ Left	Front ↔ Right	Front ↔ Back	Left ↔ Right	Left ↔ Back	Right ↔ Back
Distance (μm)		293	343	320	330	343	293
Pearson's r	Experiment #1	0.0376	0.0695	0.0317	0.05	0.0224	0.0414
	Experiment #2	0.0214	0.0539	0.0432	0.0179	0.0359	0.0161
	Experiment #3				0.0586		
Single-sided neural probe							
Recording electrode pair		1 ↔ 2	1 ↔ 3	1 ↔ 4	2 ↔ 3	2 ↔ 4	3 ↔ 4
Distance (μm)		200	215	90	70	215	200
Pearson's r	Experiment #1	0.7455	0.7472	0.7467	0.7465	0.7457	0.7475
	Experiment #2	0.6019		0.4641		0.5733	
	Experiment #3				0.5487	0.8084	0.5832

3.4.2 *In vivo* Electrical Stimulation Experiments

The result of *in vivo* electrical stimulation experiments using the LCP-based depth-type stimulation electrode is shown in Figure 3.22. As the result of stimulating MFB through the electrode channels of the fabricated stimulation electrode, the trained experimental rats press the lever to get the reward stimulation delivered from the inserted stimulation electrode. According to the results, it is confirmed that the stimulation is delivered to the target cells through all of the front-side electrodes, back-side electrodes, and tip electrodes. The results also demonstrate the feasibility of the fabricated EIROF electrodes as stimulated electrodes.

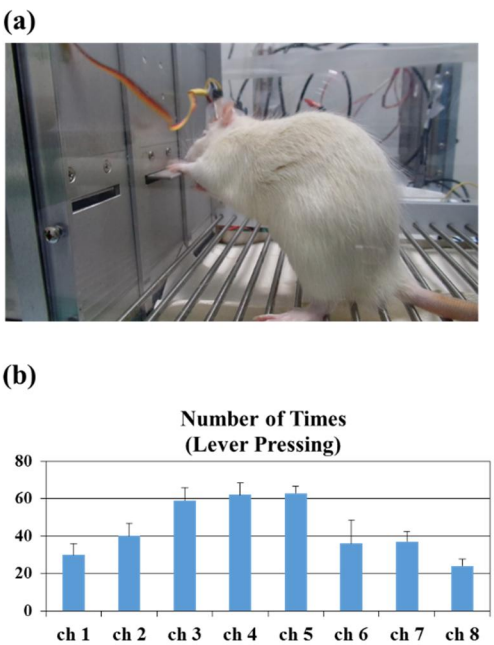

Figure 3.22 Experimental results of *in vivo* stimulation experiments using the LCP-based depth-type stimulation electrode. (a) Trained experimental rat presses a lever to get the reward stimulation delivered from the implanted electrodes. (b) Number of lever pressing by stimulation of each channel of the depth-type stimulation

electrode.

Using the developed EIROF as an electrode material, neuronal activities are also recorded from the rat brain with neuropathic pain. The electrodes are positioned onto the VPL and the cold stimulus evokes neuronal responses. According to the previous study, pain can be evoked by a cold stimulus in the neuropathic pain (cold allodynia) model, generating ectopic discharges in the VPL [39]. It was also reported that the cold pain can be suppressed by electrical stimulation on the VPL [39], [101]. In order to show the feasibility of the proposed electrode, electrical stimulation is delivered and the neural response is recorded via the electrodes in the neuropathic pain model while acetone evoked cold pain. The cold stimulus evokes a rapid change of the local field potential of the VPL (Figure 3.23 (a)). However, the local field potential is scarcely changed by the electrical stimulation of the VPL (Figure 3.23 (b)). Furthermore, the baseline amplitude of the field potential in the VPL is found to be higher after the electrical stimulation than in the resting state (without electrical stimulation). It can be assumed that this higher background activity is generated by electrical stimulation. In some previous reports, it was found that pain suppression by electrical stimulation was maintained for at least 30 min [99], [101]. In the recording results, the same tendency is demonstrated. The exaggerated baseline activity is reduced within minutes.

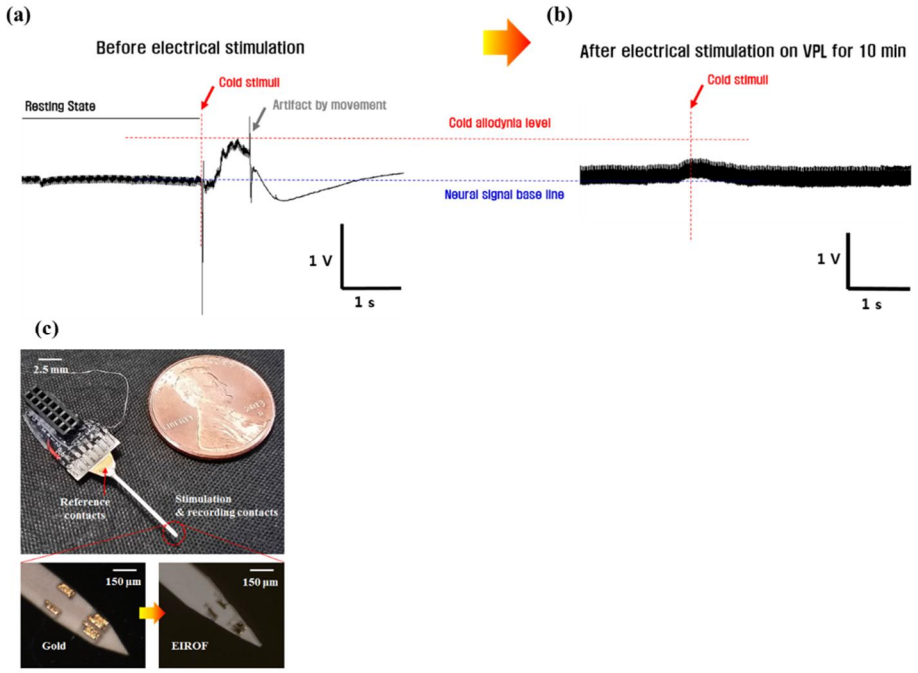

Figure 3.23 Results of *in vivo* neural stimulation and recording experiments: (a) neural response before electrical stimulation and (b) changed neural response after electrical stimulation on ventral posterolateral nucleus (VPL) for 10 min. (c) The used LCP-based deep brain stimulation electrode with EIROF electrode sites.

3.4.3 *In vivo* Optical Stimulation and Electrical Recording Experiments

The results of *in vivo* optical stimulation through optic fiber and electrical recording using the fabricated tetrodes are shown in Figure 3.24 and Figure 3.25. Using the LCP-based tetrode, spontaneous activities and light stimulation evoked neural signals are successfully recorded.

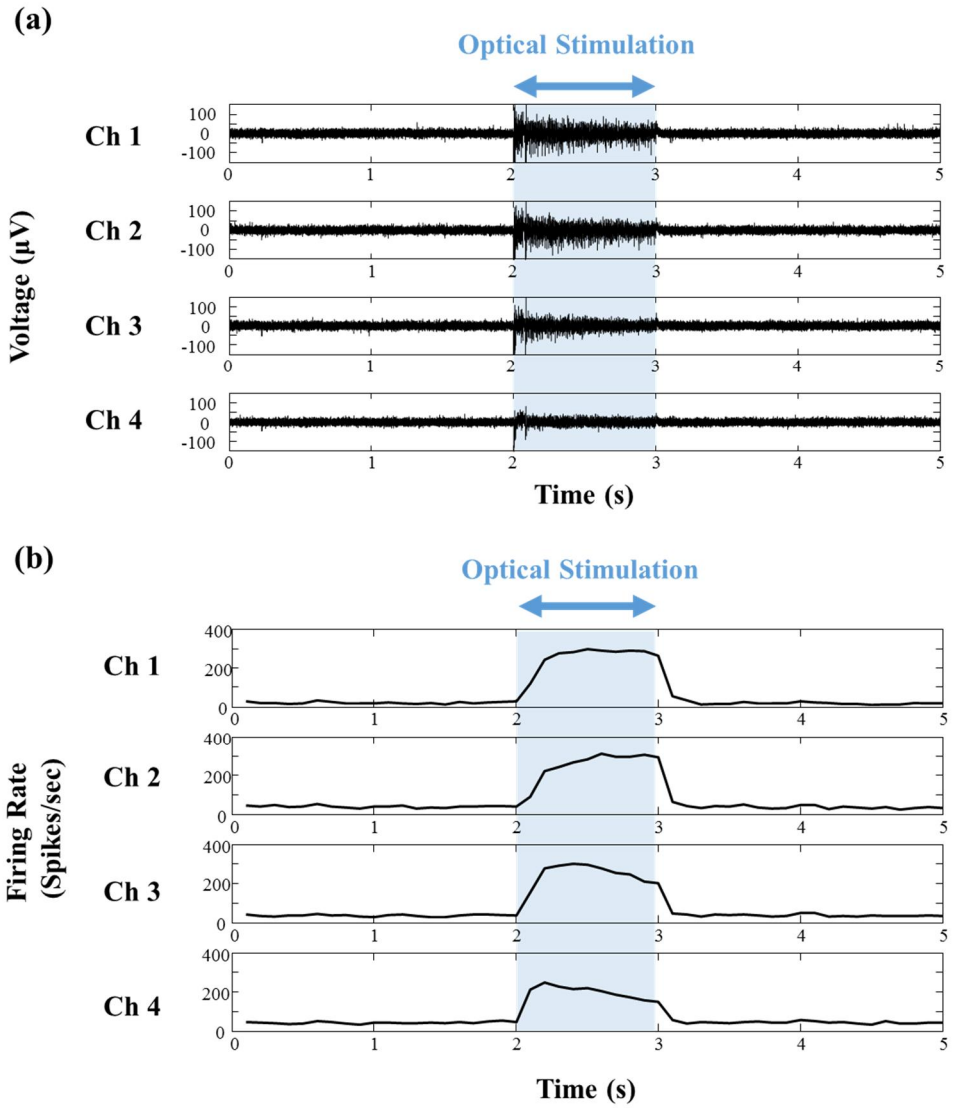

Figure 3.24 Experimental results of *in vivo* optical stimulation and electrical recording using the LCP-based tetrode: (a) raw traces and (b) peri-stimulus time histogram (PSTH).

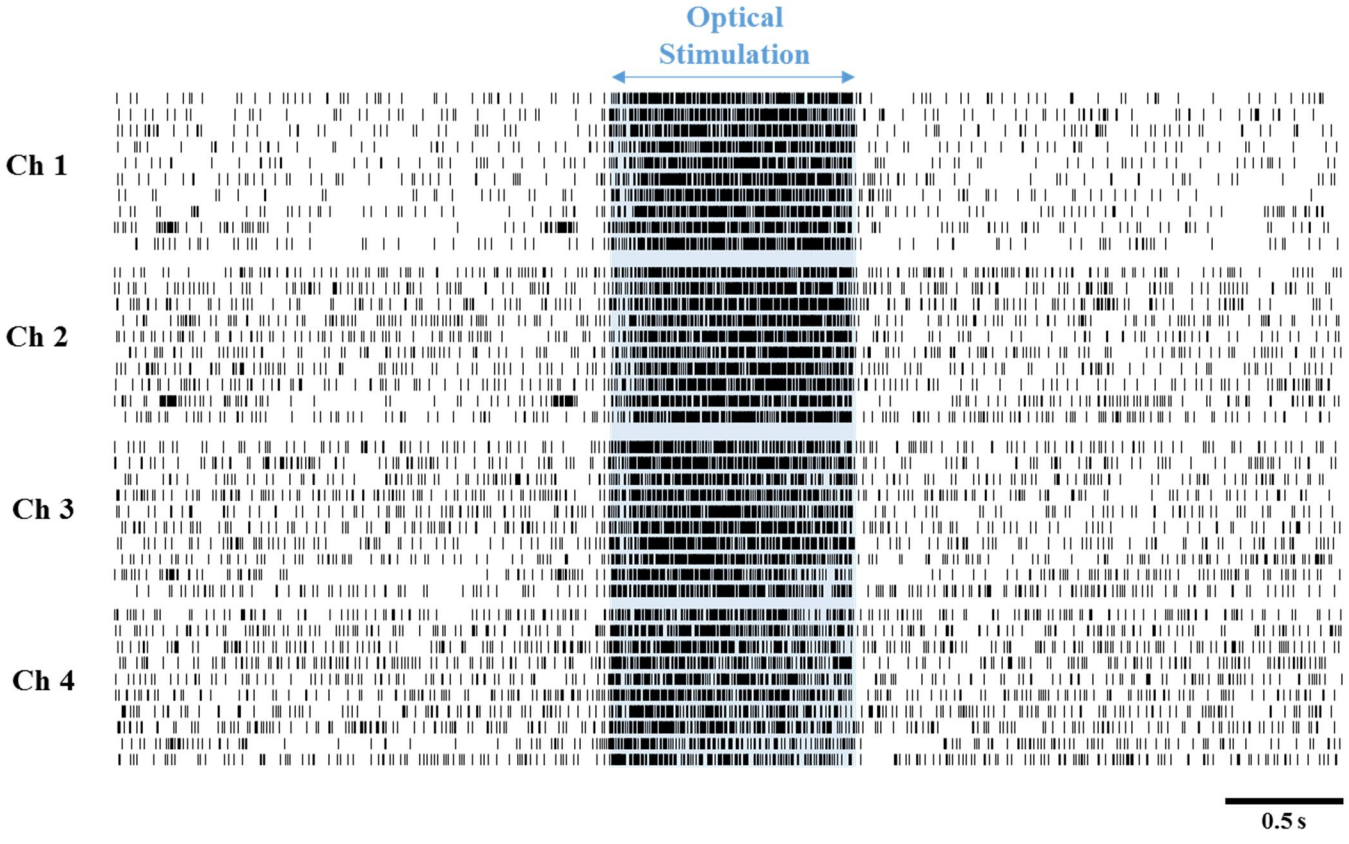

Figure 3.25 Experimental results of *in vivo* optical stimulation and electrical recording using the LCP-based tetrode: the raster plot.

The results of *in vivo* optical stimulation electrical recording using the fabricated LCP-based optrodes are shown in Figure 3.26, Figure 3.27, Figure 3.28, and Figure 3.29. Using the LCP-based optrode, spontaneous activities and light stimulation evoked neural signals are successfully recorded. Since the fabricated optrode has integrated optic fiber, optical stimulation and neural signal recording are possible in deep brain area as well as cortex of the experimental animals. Figure 3.26 and Figure 3.27 are the results of *in vivo* optical stimulation electrical recording at the posterior parietal cortex (Insertion depth: 699 μm). And Figure 3.28 and Figure 3.29 are the results of *in vivo* optical stimulation electrical recording at the hippocampus (Insertion depth: 1714 μm).

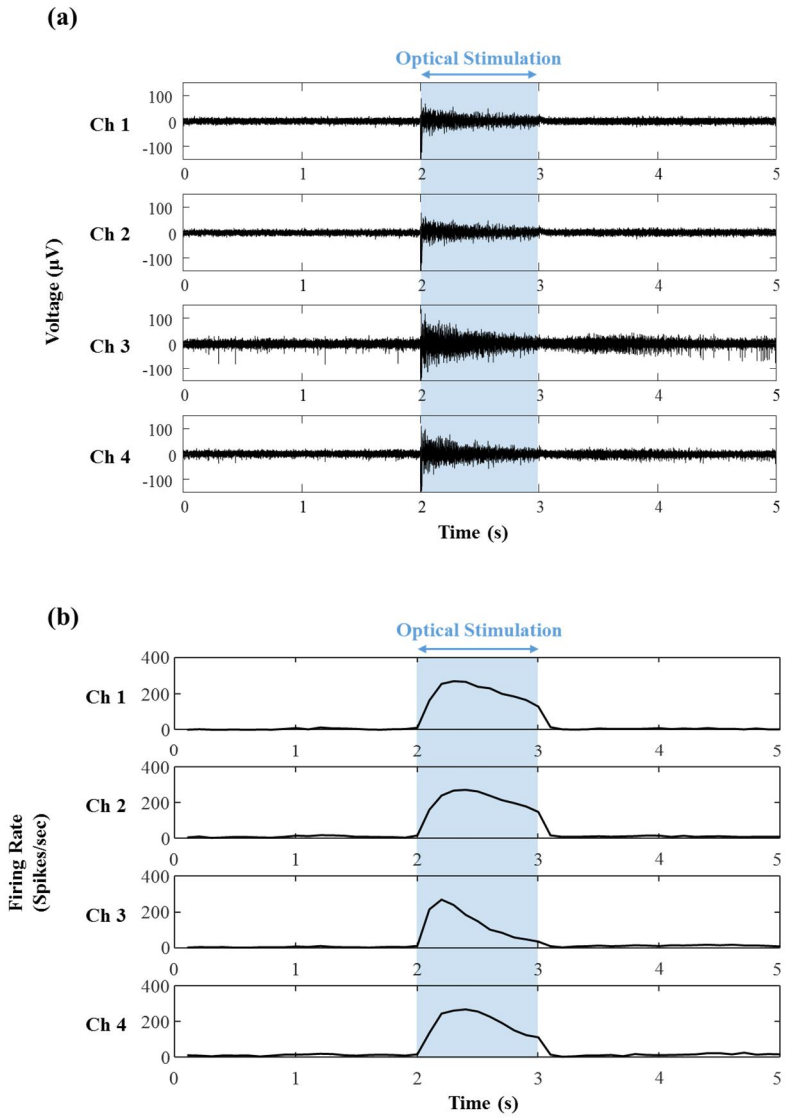

Figure 3.26 Experimental results of *in vivo* optical stimulation and electrical recording using the LCP-based optrode inserted at the posterior parietal cortex (Insertion depth: 699 μm): (a) raw traces and (b) peri-stimulus time histogram (PSTH).

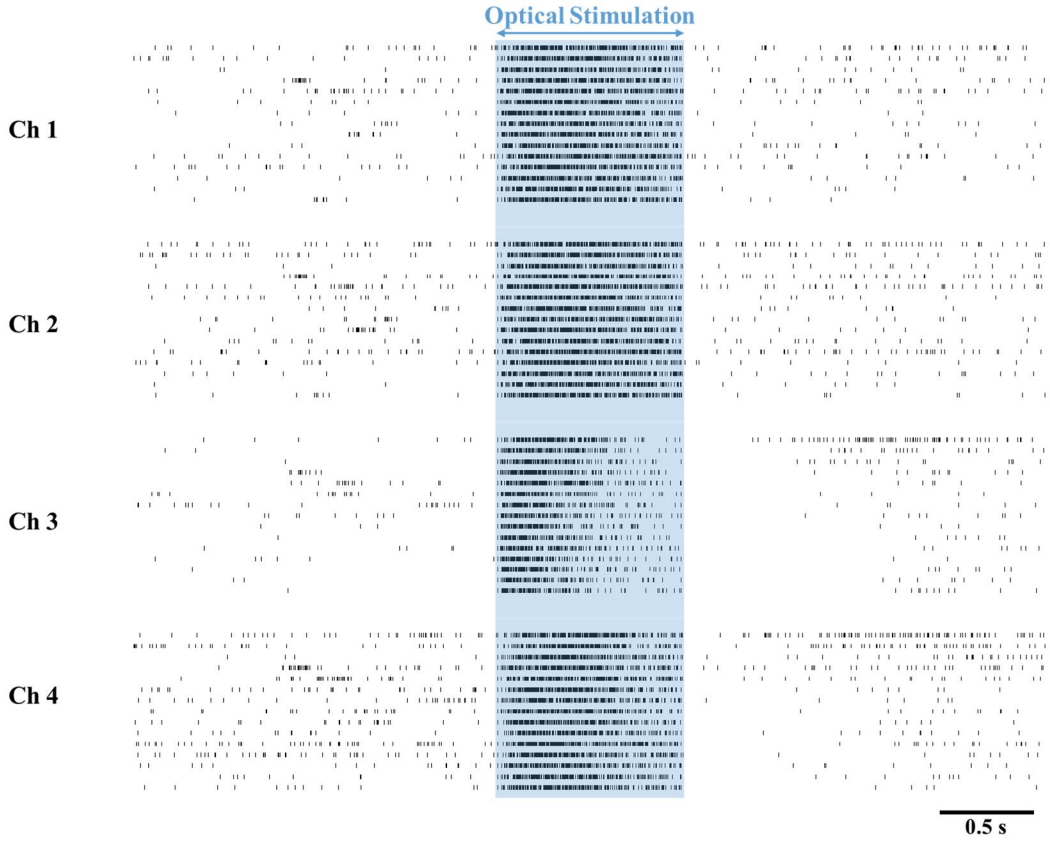

Figure 3.27 Experimental results of *in vivo* optical stimulation and electrical recording using the LCP-based optrode inserted at the posterior parietal cortex (Insertion depth: 699 μm): the raster plot.

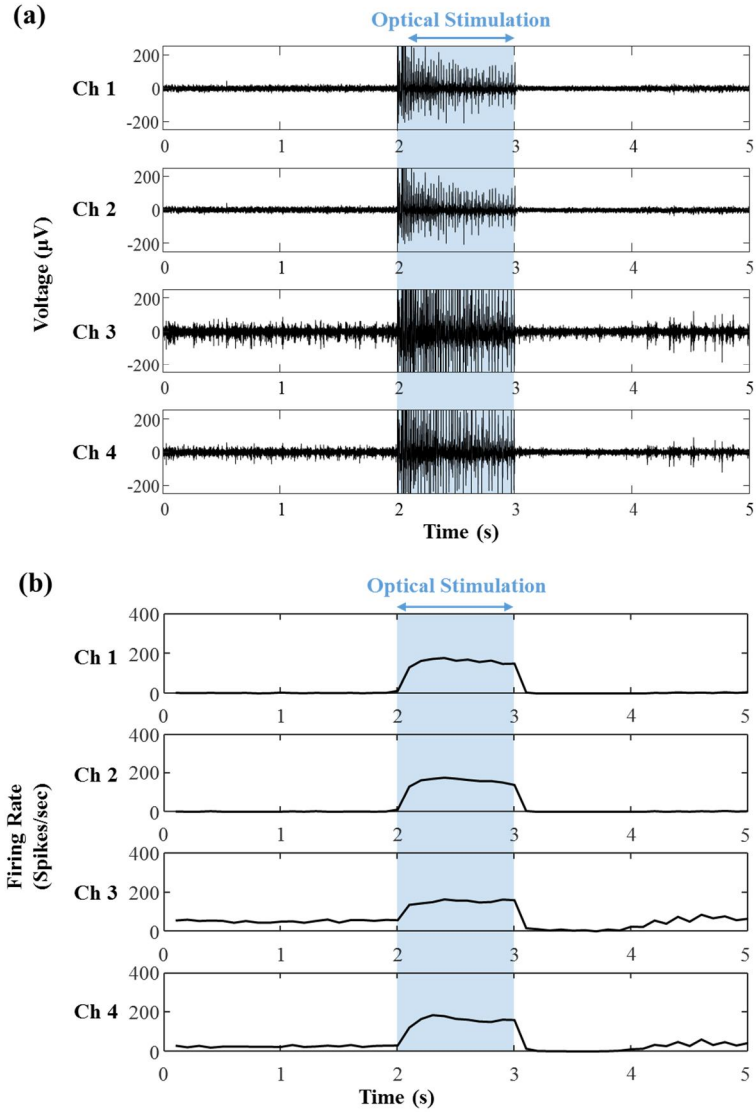

Figure 3.28 Experimental results of *in vivo* optical stimulation and electrical recording using the LCP-based optrode inserted at the hippocampus (Insertion depth: 1714 μm): (a) raw traces and (b) peri-stimulus time histogram (PSTH).

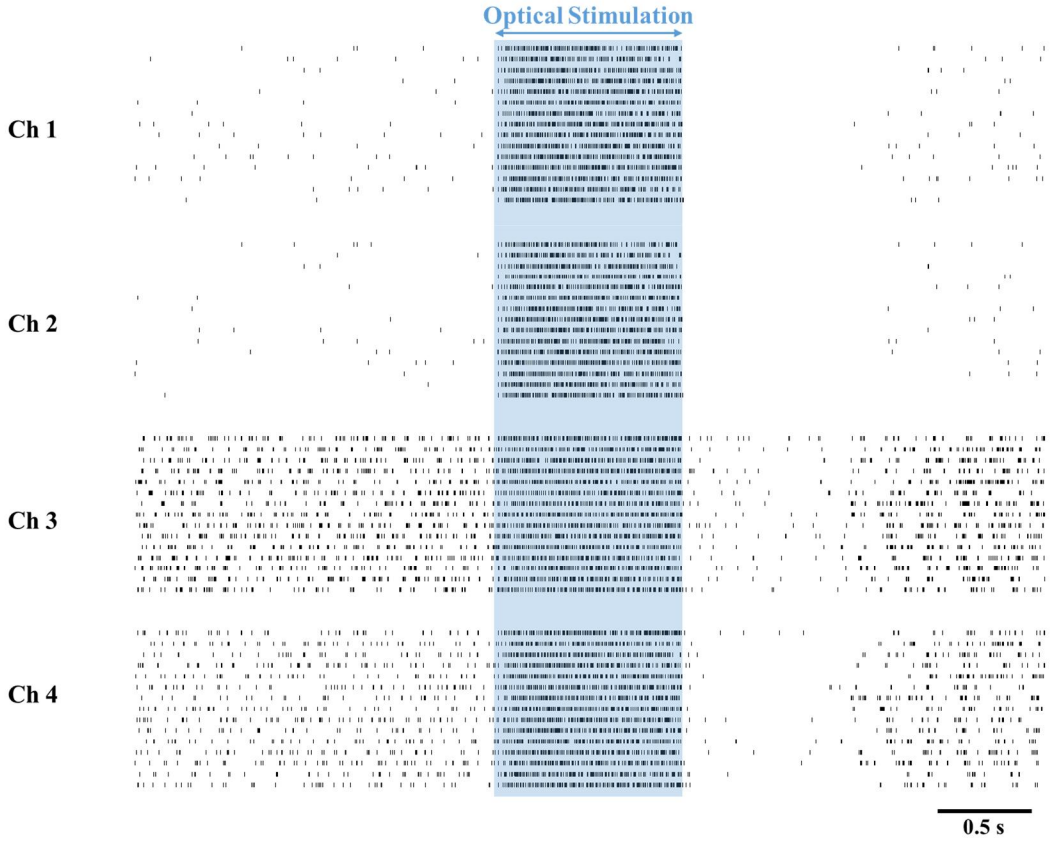

Figure 3.29 Experimental results of *in vivo* optical stimulation and electrical recording using the LCP-based optrode inserted at the hippocampus (Insertion depth: 1714 μm): the raster plot.

Chapter IV

Discussion

4.1 LCP-based Recording Probes

In this study, a novel four-sided neural probe is fabricated using LCP and its functionalities are verified *in vivo*. The LCP-based four-sided neural probe is fabricated by a thermal lamination process involving multiple LCP films and a laser micromachining process. The advantages of this four-sided neural probe are its simple fabrication process and the potential for 3-D *in vivo* neural signal recording.

The multilayered thermal lamination process and laser micromachining process are used to form three-dimensionally distributed electrodes. The thickness of the neural probe is determined by the number of LCP film layers used. Therefore, if using one LCP film for the metal-patterned layer and one for the cover layer, the thickness of the neural probe will be 50 μm. Moreover, the width of the neural probe is determined by the margin needed for the laser micromachining process. Current fabrication technology requires at least a 100-μm margin for both the right and left sides of the metal line in the laser micromachining process, and a 20-μm-thick metal line is used. Therefore, if a single-channel neural probe is made, the corresponding thickness and width of the probe will be 50 and 220 μm, respectively. Also a 16-channel neural probe can be fabricated while maintaining the thickness and width of the electrode shank at the current values (thickness: 150 μm, width: 350 μm). With respect to the number of channels and the size of the shank, the neural probe proposed here has not achieved the level of integration already achieved by its silicon-based counterparts. However, the proposed neural

probe has the advantage of being able to position the electrodes on all four sides of the shank. In terms of tissue damage caused by the insertion of the probe, the reduction of the size of the neural probes would be an important issue. Ultimately, it would be beneficial to fabricate a four-sided neural probe with a smaller-sized shank with a plurality of channels.

In addition, the short-term soak test (10 days, 75 °C) results show that the electrical interconnections of the fabricated neural probes are maintained. After the short-term soak test, delamination is not observed in the LCP layers, and the state of the neural probes is identical to that before the soak test. Although the soak test is a short-term experiment, its results lend support to the long-term implantable features of the LCP-based neural prostheses, as also shown in our previous long-term soak test studies [33] , [77], [80].

In addition, crosstalk through the recording path between adjacent recording electrode channels is theoretically analyzed [104]. Crosstalk can theoretically be analyzed by modeling the various impedances involved in the recording path. Figure 4.1 shows an equivalent circuit of two parallel metal lead lines connecting two adjacent recording electrode channels. It is assumed that the electrochemical impedances and the input impedances for the neural amplifier of two adjacent channels are the same. Metal lead lines of the same length and width also assumed. In this model, $Z_{electrode}$ represents the electrochemical impedance of electrode channel, $Z_{crosstalk}$ the coupling impedance between the two metal lead lines, Z_{sh} the wire shunt of parasitic impedance to ground, and Z_L the input impedance of the subsequent neural amplifier (recording system). The crosstalk

model between the input of channel number 1(ch1) and the output of channel number 2 (ch2) can be illustrated as Figure 4.2.

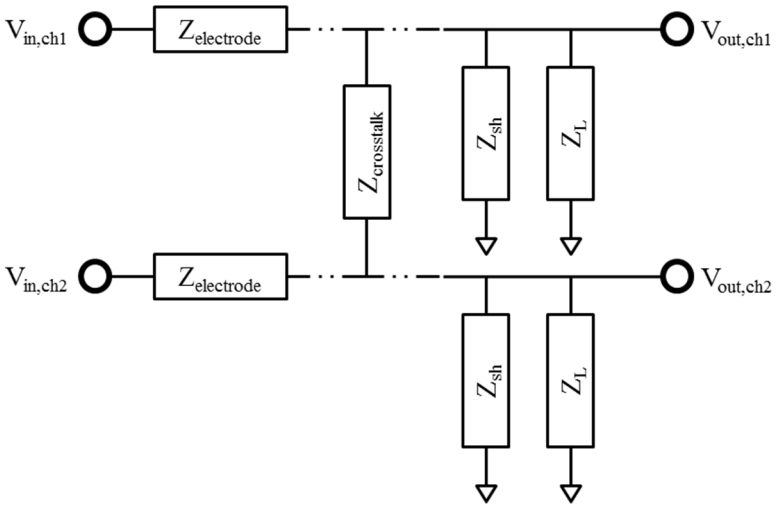

Figure 4.1 Equivalent circuit of two parallel metal lead lines connecting two adjacent recording electrode channels.

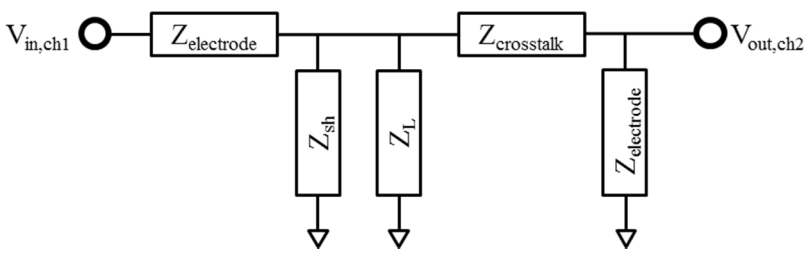

Figure 4.2 Crosstalk model of from input of channel number 1 ($V_{in,\ ch1}$) to output of channel number 2 ($V_{out,ch2}$).

Typically, Z_{sh} and Z_L each have a large value, ranging from tens to hundreds of mega-ohms and dozens to tens of mega-ohms. Since the electrochemical impedance of the recording electrode channel ($Z_{electrode}$) is several hundreds of kilo-ohms, it has a very small value compared with Z_L and Z_{sh}. ($Z_L \gg Z_{electrode}$ and $Z_{sh} \gg Z_{electrode}$) We can calculate the crosstalk between $V_{in,\ ch1}$ and

$V_{out,ch2}$ as [105]:

$$\text{Crosstalk (dB)} = -20 \log\left(\frac{V_{in,ch1}}{V_{out,ch2}}\right)$$

$$\approx -20 \log(2 + \frac{Z_{crosstalk}}{Z_{electrode}} + \frac{Z_{crosstalk}}{Z_{sh} \parallel Z_L})$$

$$(\because Z_{sh} \gg Z_{electrode} \; and \; Z_L \gg Z_{electrode})$$

The crosstalk impedance required to calculate the crosstalk in the previous formula can be defined as:

$$Z_{crosstalk} = \frac{1}{2\pi f C_{crosstalk}}$$

.At this time, the metal lead line of the adjacent recording channels of the fabricated electrode can be modeled as a parallel plate capacity. The parallel plate capacitance is determined by the following formula from the dielectric constant of the dielectric material when two conductive plates with a cross-sectional area of A are separated by a distance of d and a dielectric substance in between:

$$\mathrm{C} = \frac{(\varepsilon_r \varepsilon_0)A}{d}$$

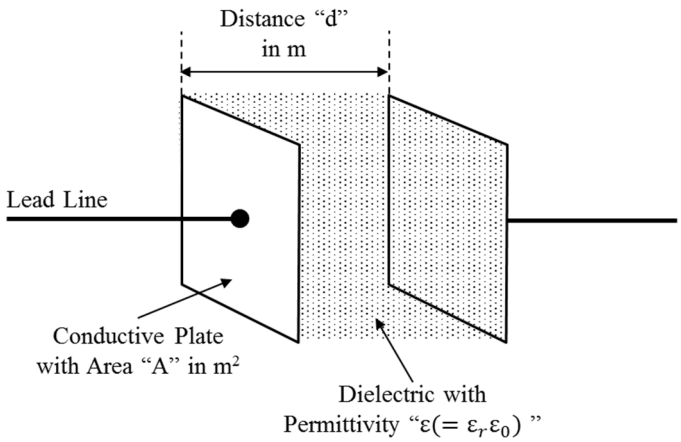

Figure 4.3 Parallel plate capacitor.

The distance between the adjacent metal lead lines of the single-sided neural probe and the four-sided neural probe and the area of the cross section are as follows. First, the single-sided neural probe is made with a metal patterned LCP layer having 20 μm spacing and 20 μm width lead line-patterns. As a result, the cross-sectional area of the two adjacent metal lead lines in the single-sided neural probe is multiplied by the length of the shank of 10 mm and the plating height of 5 μm, and the distance between the two lead lines is 20 μm. The four-sided neural probe is fabricated with thermal lamination of 25-μm-thick LCP films patterned with metal lines with a height of 5 μm and a width of 20 μm. In other words, the two closest channels have the same spacing of 20 μm as the four-sided neural probe. As a result, the cross-sectional area of the two adjacent metal lead lines in the four-sided neural probe is calculated as the product of the length of the shank of 10 mm and the width of the lead line, which is 20 μm. The gap between the two lines is 20 μm.

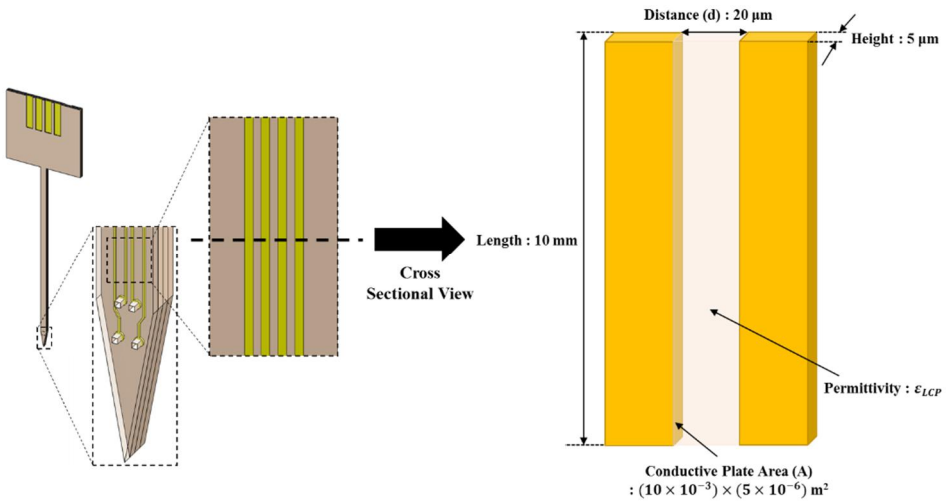

Figure 4.4 Cross-sectional area of the two adjacent metal lead lines in the single-sided neural probe.

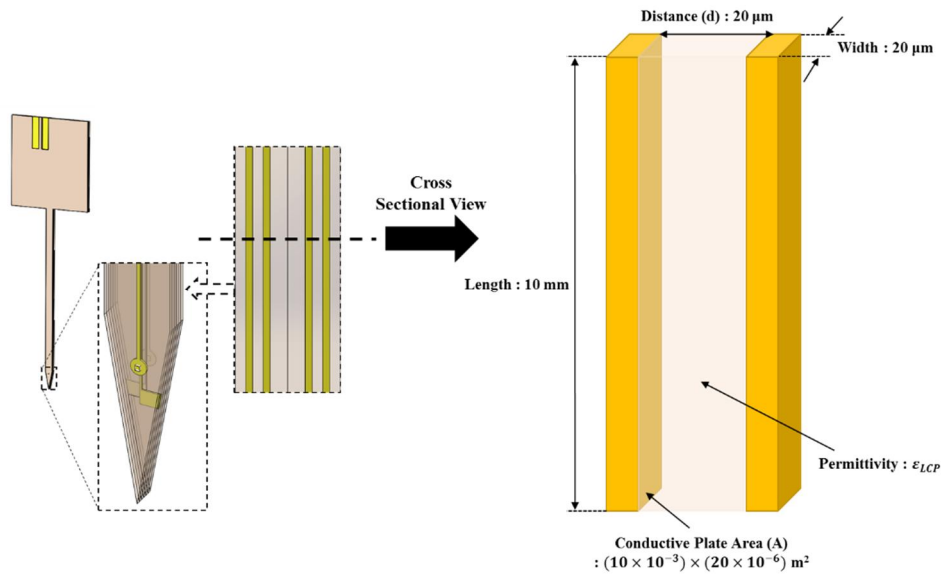

Figure 4.5 Cross-sectional area of the two adjacent metal lead lines in the four-sided neural probe.

The relative permittivity of LCP has an average value of 3 [86]. The permittivity of the LCP is calculated using the formula:

$$\varepsilon_{LCP} = \varepsilon_{r\_LCP} \times \varepsilon_0$$

$$= 3 \times (8.85 \times 10^{-12})$$

$$= 26.55 \times 10^{-12}\ [F/m]$$

The crosstalk capacitance between the adjacent metal lead lines is calculated to be 0.2655 pF for the four-sided neural probe and 0.06638 pF for the single-sided neural probe:

$$C_{crosstalk\_four-sided} = \frac{(\varepsilon_{LCP})A_{four-sided}}{d_{four-sided}}$$

$$= \frac{(26.55 \times 10^{-12})(20 \times 10^{-6} \times 10 \times 10^{-3})}{(20 \times 10^{-6})}$$

$$= 0.2655\ \text{pF}$$

$$C_{crosstalk\_single-sided} = \frac{(\varepsilon_{LCP})A_{single-sided}}{d_{single-sided}}$$

$$= \frac{(26.55 \times 10^{-12})(5 \times 10^{-6} \times 10 \times 10^{-3})}{(20 \times 10^{-6})}$$

$$= 0.06638\ \text{pF}$$

From this, the crosstalk impedance is calculated as 0.6 GΩ for the four-sided neural probe and 2.4 GΩ for the single-sided neural probe:

$$Z_{crosstalk\_four-sided} = \frac{1}{2\pi f C_{crosstalk\_four-sided}}$$

$$= \frac{1}{2\pi(1 \times 10^3)(0.2655 \times 10^{-12})}\ (at\ 1kHz)$$

$$= 0.6\ \text{GΩ (at 1kHz)}$$

$$Z_{crosstalk\_single-sided} = \frac{1}{2\pi f C_{crosstalk\_single-sided}}$$

$$= \frac{1}{2\pi(1 \times 10^{3})(0.06638 \times 10^{-12})}\ (at\ 1kHz)$$

$$= 2.4\ \text{GΩ (at 1kHz)}$$

Let's assume the values of Z_{sh} and Z_L as 10 MΩ and $Z_{electrode}$ as 300 kΩ (the average value of the fabricated recording electrodes). Therefore, the crosstalk between the adjacent recording channels is calculated as -66.53 dB for the four-sided neural probe and -75.87 dB for the single-sided neural probe:

$$Crosstalk_{four-sided}\ (dB)$$

$$= -20\ \log(2 + \frac{Z_{crosstalk\_four-sided}}{Z_{electrode}} + \frac{Z_{crosstalk\_four-sided}}{Z_{sh}\ \|\ Z_L})$$

$$= -66.53\ \text{dB}$$

$$Crosstalk_{single-sided}\ (dB)$$

$$= -20\ \log(2 + \frac{Z_{crosstalk\_single-sided}}{Z_{electrode}} + \frac{Z_{crosstalk\_single-sided}}{Z_{sh}\ \|\ Z_L})$$

$$= -78.57\ \text{dB}$$

As 1% of crosstalk, which is -40 dB, is considered as "considerable crosstalk" [104], [105], both the four-sided and single-sided neural probes appear not to cause crosstalk in the adjacent recording path.

The functionality of the novel neural probe is demonstrated by *in vivo* animal experiments. As in other 3-D neural probe studies [4]-[9], [11]-[15], [18]-[21], [24]-[26], [28]-[30], we records *in vivo* neural signals; we used the proposed four-sided neural probe to record neural signals from various cells and compared these signals with the signals recorded using a single-sided neural probe. These *in vivo* studies demonstrate that various signals from a complex neural network can be recorded using three-dimensionally distributed electrodes, which is difficult to achieve using single-sided electrodes.

For decades, microwire-based tetrodes have been widely and usefully used for *in vivo* neural signal recording experiments. The advantage of microwire-based tetrodes among various neural electrode arrays is that its structure allows electrode sites to have easy access to nearby intact neurons. However, the fabrication process of the microwire-based tetrodes requires a mastery of manual skills and the resulting device tends to be unregulated. The novel neural probe developed in this study has four electrodes—one on each of the four sides of a single electrode shank. The proposed LCP-based fabrication processes can be used to layer many different types of electrodes onto one shank of the probe. Thus, neural probe with electrodes aligned at the tip of the electrode shank is also developed and named it as LCP-based tetrode. This design is proposed as a design that applies the structural advantages of the microwire-based tetrode, which may be advantageous for collecting neural signals from intact neurons. The suggested LCP-based tetrodes can be exquisitely fabricated by micro-fabrication processes and laser micromachining. And its use has been proven by through *in vivo* neural signal

recording tests.

4.2 LCP-based Depth-type Stimulation Electrode

The concept and fabrication methodology of LCP-based neural probes for recording are applicable to neural stimulation experiments. Moreover, the number of channels can be increased by increasing the number of LCP layers formed during the multilayered thermal lamination process, by increasing the number of electrodes, or by changing the pattern of electrodes on one piece of the LCP film. Therefore, LCP-based depth-type simulation electrode with multi-sided electrode channels are developed. The suggested depth-type stimulation electrode has three electrode channels each on the front and back side and two at the tip of the electrode shank.

For stimulation, EIROF are formed on gold surfaces by application of triangular voltage waveforms followed by rectangular pulses in electrodeposition solution for iridium oxide. In order to investigate the effects of the triangular waveforms and the rectangular pulses on formation of EIROFs, different numbers of triangular waveforms and rectangular pulses are applied during the electrodeposition. Then the electrochemical and the mechanical characteristics of the formed EIROF electrodes are analyzed.

As the number of rectangular pulses increases, the charge storage capacity increases, whereas the electrochemical impedance is not affected. This is consistent with the results of SEM and XPS. SEM images confirmed that the surface morphologies of the EIROFs are similar even after different numbers of rectangular

pulses as shown in Figure 4.1. However, the XPS results indicates higher iridium content in EIROFs with the increased number of rectangular pulses (Figure 4.2). As a result, the electrochemical impedance do not change because the porosity of the EIROF is not affected by the number of rectangular pulses, whereas the charge storage capacity increases due to the higher atomic content of iridium.

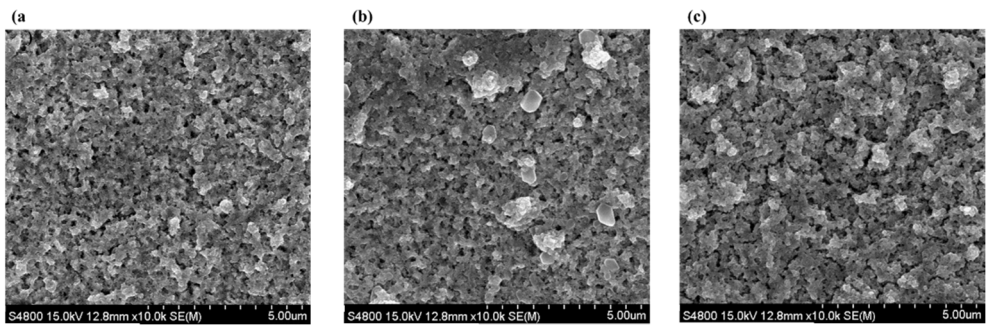

Figure 4.6 SEM images of EIROFs made with different numbers of repetitions of rectangular pulses; the numbers of rectangular pulses were (a) 1800, (b) 3600, and (c) 5400 (number of triangular waveforms: 50).

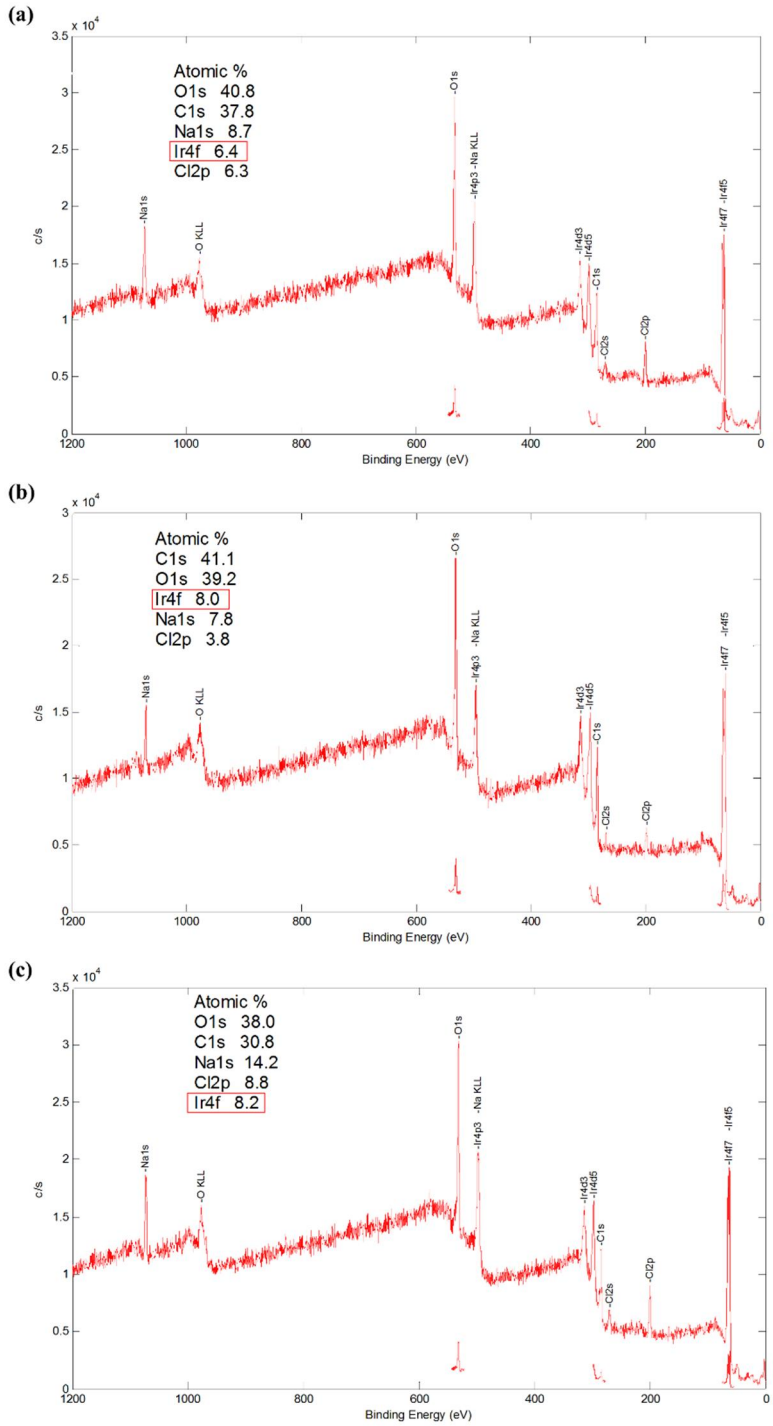

Figure 4.7 XPS measurements of EIROFs formed with different numbers of repetitions of the rectangular pulses; the numbers of rectangular pulses were (a) 1800, (b) 3600, and (c) 5400 (number of triangular waveforms: 50).

Unlike the rectangular pulses, the number of triangular waveforms do not affect either the electrochemical impedance or the charge storage capacity. However, it appears that the number of triangular waveforms is related to the mechanical stability of EIROFs. Even though the taping test do not show any meaningful change before and after the taping process, the sonication test results in different electrochemical characteristics and the surface morphologies of EIROFs after sonication as shown in chapter 3.2. Regardless of the number of triangular waveforms, the sonication obviously induces an increase in the electrochemical impedances and a decrease in the charge storage capacities as shown in Table 4.1. XPS analysis shows the results of different numbers of triangular waveforms in terms of the iridium compositions at the electrode surface. The composition of iridium decreases much more for the EIROFs formed using fewer triangular waveforms. It is likely that the triangular waveforms initiate the slower deposition of iridium oxide, which is advantageous for electroplating, especially on the different surface. The quantitative XPS results support that an increase in the number of triangular waves can make the surfaces of EIROFs stronger and more stable.

The charge-injection limits for iridium oxide films (AIROF) on iridium wires are reportedly ±2 mC/cm^2 for the anodic current and ±1 mC/cm^2 for the cathodic, respectively [103]. For iridium oxide films (SIROF) made from sputtered iridium metal, the charge-injection limit is reported to be 4−6 mC/cm^2 [46]. The measured charge-injection limit of the fabricated electrodeposited iridium oxide film 1.27 mC/cm^2. It may not be appropriate to directly compare the values from

different research groups since the conditions for the measurements, such as electrolyte compositions, pulse width, reference electrode, electrode size, and to forth could be different. However, the proposed EIROF has a charge-injection limit comparable to the values in the literature. More importantly, the feasibility of the proposed EIROF electrode is successfully shown using *in vivo* recording from rats.

Table 4.1 Averaged electrochemical characteristics of gold and EIROFs for various electrodeposition protocols, with the averaged electrochemical characteristics of EIROFs measured after the sonication tests (LCP-based microelectrodes with a radius of 150 μm) (The number of triangular waveforms was varied from 50, 100, 200, to 400; the number of rectangular pulses was varied from 1800, 3600, to 5400).

		Electrochemical impedance at 1 kHz (kΩ)	Cathodic charge storage capacity (CSC_C) (mC/cm^2)
Gold		26.65 ± 6.93	0.32 ± 0.05
EIROF	Before the sonication tests	1.41 ± 1.1	24.19 ± 6.21
	After the sonication tests	2.16 ± 2.12	7.43 ± 1.72

4.3 LCP-based Optrode

In this study, a LCP-based optrode is also developed and its functionalities are verified through *in vivo* optical stimulation and neural signal recording experiments. The fabricated optrode has four recording electrodes at the tip of the

electrode shank and integrated optic fiber for light stimulation.

LCP-based neural probe fabrication techniques are used to create LCP-based tetrode of the same structure as microwire-based tetrode. And the LCP-based optrode is made by integrating an optic fiber with the LCP-based tetrode. The *in vivo* experiment results show that the fabricated LCP-based optrode can be applied to the cortex as well as the deep brain area. According to the results, it is expected that various optrodes can be made by considering a 3-D neural structure.

Chapter V

Conclusion

In the present study, novel LCP-based neural probes including four-sided neural probe, tetrode, stimulation electrode with multi-sided electrode sites, and optrode are reported. The neural probes with multi-sided electrodes including four sides and tip of the electrode shank are developed using a thermal lamination process involving multiple LCP layers and laser micromachining.

The developed four-sided neural probe has four recording electrodes on the front, back, and two sidewalls of the electrode shank. According to *in vivo* recordings in the mouse somatosensory cortex, the single-sided neural probe collects a considerably larger number of identical spikes patterns than the four-sided neural probe. Also, the pair-wise Pearson correlation coefficient analysis and cross-correlation analysis results show that the single-sided neural probe recorded higher correlated neural signals than the four-sided neural probe. As the results, the four-sided neural probe can record diverse neural activities simultaneously as compared to the single-sided probe.

In this presentation, the LCP-based tetrode mimicking the structure of a microwire-based tetrode is fabricated by micro-fabrication processes. As the result, the dimensions in the fabricated tetrodes are well controlled and the devices are mass producible. The suggested neural probes have four contacts at the tip by the developed fabrication involves bonding multiple layer LCP films by thermal lamination and exposing electrode sites by laser micromachining.

In general, effective electrical stimulation of the nerve system necessitates delivering a large amount of charge to the target neurons. To date, iridium oxide is one of the most effective materials due to its superior electrochemical

characteristics for neural stimulation. In this study, the depth-type stimulation electrode with EIROF is developed using LCP. The roles of triangular waveforms and rectangular pulses are confirmed in terms of the surface adhesion strength and charge-storage capacity. An increase in the number of triangular waves increases the mechanical stability of EIROF, while the increase in the number of rectangular pulses increases the charge storage capacity of EIROFs. Finally, the feasibility of a LCP-based depth-type stimulation electrode with the proposed EIROF electrode sites is verified in an *in vivo* experiment. The developed stimulation electrode has electrode channels on the front and back side and at the tip of the electrode shank. Therefore, the results of animal experiments also show the usefulness of the fabricated electrodes with electrode channels on multiple sides of the shank as stimulating electrodes. The LCP-based multi-sided stimulation electrode with the EIROF is expected to become a key technology for neural prostheses in the near future.

In addition to the use of electrical stimulation and electrical recording, recently optrodes for optical stimulation and electrical recording have been widely researched. Therefore, LCP-based optrode is developed for optogenetic researches. By integrating optic fiber with the LCP-based tetrode, the LCP-based optrode is developed and can be applied to both the cortex and the deep brain area. The effectiveness of the fabricated optrodes is confirmed by the *in vivo* experiments. It is expected that future LCP-based optrode can be used for various optogenetic experiments by taking advantage of LCP-based neural probes which are easy to make electrode channels on multi sides of the electrode shank.

References

[1] J. Skrzypek, and E. Keller, "Manufacture of metal microelectrodes with the scanning electron microscope," *IEEE Trans Biomed Eng,* vol. 22, no. 5, pp. 435-7, Sep, 1975.

[2] P. K. Campbell, K. E. Jones, R. J. Huber, K. W. Horch, and R. A. Normann, "A silicon-based, three-dimensional neural interface: manufacturing processes for an intracortical electrode array," *IEEE Trans Biomed Eng,* vol. 38, no. 8, pp. 758-68, Aug, 1991.

[3] A. C. Hoogerwerf, and K. D. Wise, "A three-dimensional microelectrode array for chronic neural recording," *IEEE Trans Biomed Eng,* vol. 41, no. 12, pp. 1136-46, Dec, 1994.

[4] Q. Bai, K. D. Wise, and D. J. Anderson, "A high-yield microassembly structure for three-dimensional microelectrode arrays," *IEEE Trans Biomed Eng,* vol. 47, no. 3, pp. 281-9, Mar, 2000.

[5] T. H. Yoon, E. J. Hwang, D. Y. Shin, S. I. Park, S. J. Oh, S. C. Jung, H. C. Shin, and S. J. Kim, "A micromachined silicon depth probe for multichannel neural recording," *IEEE Trans Biomed Eng,* vol. 47, no. 8, pp. 1082-7, Aug, 2000.

[6] I. Ulbert, E. Halgren, G. Heit, and G. Karmos, "Multiple microelectrode-recording system for human intracortical applications," *J Neurosci Methods,* vol. 106, no. 1, pp. 69-79, Mar 30, 2001.

[7] P. J. Rousche, D. S. Pellinen, D. P. Pivin, J. C. Williams, R. J. Vetter, and D. R. Kipke, "Flexible polyimide-based intracortical electrode arrays with bioactive capability," *Ieee Transactions on Biomedical Engineering,* vol. 48, no. 3, pp. 361-371, Mar, 2001.

[8] K. C. Cheung, K. Djupsund, Y. Dan, and L. P. Lee, "Implantable multichannel electrode array based on SOI technology," *Journal of Microelectromechanical Systems,* vol. 12, no. 2, pp. 179-184, Apr, 2003.

[9] S. J. Oh, J. K. Song, and S. J. Kim, "Neural Interface with a Silicon Neural Probe in the Advancement of Microtechnology," *Biotechnology and Bioprocess Engineering,* vol. 8, no. 4, pp. 252-256, 2003.

[10] K. Lee, A. Singh, J. P. He, S. Massia, B. Kim, and G. Raupp, "Polyimide based neural implants with stiffness improvement," *Sensors and Actuators B-Chemical,*

vol. 102, no. 1, pp. 67-72, Sep 1, 2004.

[11] S. Takeuchi, T. Suzuki, K. Mabuchi, and H. Fujita, "3D flexible multichannel neural probe array," *Journal of Micromechanics and Microengineering,* vol. 14, no. 1, pp. 104-107, Jan, 2004.

[12] H. Takahashi, J. Suzurikawa, M. Nakao, F. Mase, and K. Kaga, "Easy-to-prepare assembly array of Tungsten microelectrodes," *IEEE Trans Biomed Eng,* vol. 52, no. 5, pp. 952-6, May, 2005.

[13] T. J. Blanche, M. A. Spacek, J. F. Hetke, and N. V. Swindale, "Polytrodes: high-density silicon electrode arrays for large-scale multiunit recording," *J Neurophysiol,* vol. 93, no. 5, pp. 2987-3000, May, 2005.

[14] S. J. Oh, J. K. Song, J. W. Kim, and S. J. Kim, "A high-yield fabrication process for silicon neural probes," *IEEE Trans Biomed Eng,* vol. 53, no. 2, pp. 351-4, Feb, 2006.

[15] S. Musallam, M. J. Bak, P. R. Troyk, and R. A. Andersen, "A floating metal microelectrode array for chronic implantation," *J Neurosci Methods,* vol. 160, no. 1, pp. 122-7, Feb 15, 2007.

[16] M. HajjHassan, V. Chodavarapu, and S. Musallam, "NeuroMEMS: Neural Probe Microtechnologies," *Sensors (Basel),* vol. 8, no. 10, pp. 6704-6726, Oct 25, 2008.

[17] P. Ruther, A. Aarts, O. Frey, S. Herwik, S. Kisban, K. Seidl, S. Spieth, A. Schumacher, M. Koudelka-Hep, O. Paul, T. Stieglitz, R. Zengerle, and H. Neves, "The NeuroProbes Project - Multifunctional Probe Arrays for Neural Recording and Stimulation." p. 069.

[18] J. Du, I. H. Riedel-Kruse, J. C. Nawroth, M. L. Roukes, G. Laurent, and S. C. Masmanidis, "High-resolution three-dimensional extracellular recording of neuronal activity with microfabricated electrode arrays," *J Neurophysiol,* vol. 101, no. 3, pp. 1671-8, Mar, 2009.

[19] J. P. Seymour, N. B. Langhals, D. J. Anderson, and D. R. Kipke, "Novel multi-sided, microelectrode arrays for implantable neural applications," *Biomedical Microdevices,* vol. 13, no. 3, pp. 441-451, Jun, 2011.

[20] M. E. Merriam, S. Dehmel, O. Srivannavit, S. E. Shore, and K. D. Wise, "A 3-d 160-site microelectrode array for cochlear nucleus mapping," *IEEE Trans Biomed Eng,* vol. 58, no. 2, pp. 397-403, Feb, 2011.

[21] S. M. E. Merriam, O. Srivannavit, M. N. Gulari, and K. D. Wise, "A Three-Dimensional 64-Site Folded Electrode Array Using Planar Fabrication," *Journal of*

Microelectromechanical Systems, vol. 20, no. 3, pp. 594-600, Jun, 2011.

[22] K. Seidl, S. Herwik, T. Torfs, H. P. Neves, O. Paul, and P. Ruther, "CMOS-Based High-Density Silicon Microprobe Arrays for Electronic Depth Control in Intracortical Neural Recording," *Journal of Microelectromechanical Systems,* vol. 20, no. 6, pp. 1439-1448, 2011.

[23] B. J. Kim, C. A. Gutierrez, G. A. Gerhardt, and E. Meng, "PARYLENE-BASED ELECTROCHEMICAL-MEMS FORCE SENSOR ARRAY FOR ASSESSING NEURAL PROBE INSERTION MECHANICS," *MEMS 2012*, pp. 124-127, 2012.

[24] S. E. Lee, S. B. Jun, H. J. Lee, J. Kim, S. W. Lee, C. Im, H. C. Shin, J. W. Chang, and S. J. Kim, "A Flexible Depth Probe Using Liquid Crystal Polymer," *IEEE Transactions on Biomedical Engineering,* vol. 59, no. 7, pp. 2085-2094, Jul, 2012.

[25] I. Opris, J. L. Fuqua, P. F. Huettl, G. A. Gerhardt, T. W. Berger, R. E. Hampson, and S. A. Deadwyler, "Closing the loop in primate prefrontal cortex: inter-laminar processing," *Front Neural Circuits,* vol. 6, pp. 88, 2012.

[26] Y.-T. Lee, D. Moser, T. Holzhammer, W. Fang, O. Paul, and P. Ruther, "ULTRATHIN, DUAL-SIDED SILICON NEURAL MICROPROBES REALIZED USING BCB BONDING AND ALUMINUM SACRIFICIAL ETCHING," *MEMS 2013*, pp. 1021-1024, 2013.

[27] A. C. M. Peixoto, S. B. Goncalves, A. F. Da Silva, N. S. Dias, and J. H. Correia, "Neural Electrode Array Based on Aluminum: Fabrication and Characterization," *Ieee Sensors Journal,* vol. 13, no. 9, pp. 3319-3324, Sep, 2013.

[28] C. M. Lopez, A. Andrei, S. Mitra, M. Welkenhuysen, W. Eberle, C. Bartic, R. Puers, R. F. Yazicioglu, and G. G. E. Gielen, "An Implantable 455-Active-Electrode 52-Channel CMOS Neural Probe," *IEEE Journal of Solid-State Circuits,* vol. 49, no. 1, pp. 248-261, 2014.

[29] Z. Xiang, S.-C. Yen, N. Xue, T. Sun, W. M. Tsang, S. Zhang, L.-D. Liao, N. V Thakor, and C. Lee, "Ultra-thin flexible polyimide neural probe embedded in a dissolvable maltose-coated microneedle," *Journal of Micromechanics and Microengineering,* vol. 24, 2014.

[30] M.-Y. Cheng, L. Yao, K. L. Tan, R. Lim, P. Li, and W. Chen, "3D probe array integrated with a front-end 100-channel neural recording ASIC," *Journal of Micromechanics and Microengineering,* vol. 24, 2014.

[31] F. A. Spelman, "Cochlear electrode arrays: past, present and future," *Audiol Neurootol,* vol. 11, no. 2, pp. 77-85, 2006.

[32] K. S. Min, S. H. Oh, M. H. Park, J. Jeong, and S. J. Kim, "A polymer-based multichannel cochlear electrode array," *Otol Neurotol,* vol. 35, no. 7, pp. 1179-86, Aug, 2014.

[33] S. W. Lee, J. M. Seo, S. Ha, E. T. Kim, H. Chung, and S. J. Kim, "Development of microelectrode arrays for artificial retinal implants using liquid crystal polymers," *Invest Ophthalmol Vis Sci,* vol. 50, no. 12, pp. 5859-66, Dec, 2009.

[34] J. D. Weiland and M. S. Humayun, "Visual Prosthesis," *Proceedings of the IEEE,* vol. 96, no. 7, pp. 1076-1084, 2008.

[35] J. A. Zhou, S. J. Woo, S. I. Park, E. T. Kim, J. M. Seo, H. Chung, and S. J. Kim, "A suprachoroidal electrical retinal stimulator design for long-term animal experiments and *in vivo* assessment of its feasibility and biocompatibility in rabbits," *J Biomed Biotechnol,* vol. 2008, pp. 547428, 2008.

[36] D. B. McCreery, T. G. Yuen, W. F. Agnew, and L. A. Bullara, "Stimulation with chronically implanted microelectrodes in the cochlear nucleus of the cat: histologic and physiologic effects," *Hear Res,* vol. 62, no. 1, pp. 42-56, Sep, 1992.

[37] A. L. Benabid, "Deep brain stimulation for Parkinson's disease," *Curr Opin Neurobiol,* vol. 13, no. 6, pp. 696-706, Dec, 2003.

[38] P. S. Motta, and J. W. Judy, "Multielectrode microprobes for deep-brain stimulation fabricated with a customizable 3-D electroplating process," *IEEE Trans Biomed Eng,* vol. 52, no. 5, pp. 923-33, May, 2005.

[39] J. Kim, S. Eun Lee, K. Sik Min, H. H. Jung, J. E. Lee, S. J. Kim, and J. W. Chang, "Ventral posterolateral deep brain stimulation treatment for neuropathic pain shortens pain response after cold stimuli," *J Neurosci Res,* vol. 91, no. 7, pp. 997-1004, Jul, 2013.

[40] D. N. Rushton, "Electrical stimulation in the treatment of pain," *Disabil Rehabil,* vol. 24, no. 8, pp. 407-15, May 20, 2002.

[41] P. Shirvalkar, M. Seth, N. D. Schiff, and D. G. Herrera, "Cognitive enhancement with central thalamic electrical stimulation," *Proc Natl Acad Sci U S A,* vol. 103, no. 45, pp. 17007-12, Nov 07, 2006.

[42] A. F. DaSilva, C. Granziera, J. Snyder, and N. Hadjikhani, "Thickening in the somatosensory cortex of patients with migraine," *Neurology,* vol. 69, no. 21, pp. 1990-5, Nov 20, 2007.

[43] P. Blomstedt, U. Sandvik, A. Fytagoridis, and S. Tisch, "The posterior subthalamic area in the treatment of movement disorders: past, present, and future,"

Neurosurgery, vol. 64, no. 6, pp. 1029-38; discussion 1038-42, Jun, 2009.

[44] S. F. Cogan, "Neural stimulation and recording electrodes," *Annu Rev Biomed Eng,* vol. 10, pp. 275-309, 2008.

[45] S. A. Kim, E. T. Kim, and S. J. Kim, "Highly Efficient cold Sputtered Iridium Oxide Films for Polyimide Based Neural Stimulation Electrodes," *Journal of Biomedical Engineering Research,* vol. 30, pp. 199-204, 2009.

[46] K. Wang, C. C. Liu, and D. M. Durand, "Flexible nerve stimulation electrode with iridium oxide sputtered on liquid crystal polymer," *IEEE Trans Biomed Eng,* vol. 56, no. 1, pp. 6-14, Jan, 2009.

[47] T. Stieglitz, H. Beutel, and M. Schuettler, and J.-U. Meyer, "Micromachined, Polyimide-Based Devices for Flexible Neural Interfaces," *Biomedical Microdevices,* vol. 2, no. 4, 2000.

[48] S. F. Cogan, J. Ehrlich, T. D. Plante, A. Smirnov, D. B. Shire, M. Gingerich, and J. F. Rizzo, "Sputtered iridium oxide films (SIROFs) for neural stimulationelectrodes," *Conf Proc IEEE Eng Med Biol Soc,* vol. 6, pp. 4153-6, 2004.

[49] K. S. Kang and J. L. Shay, "Blue Sputtered Iridium Oxide Films (Blue SIROF's)," *Journal of Electrochemical Society,* vol. 130, no. 4, pp. 766-769, 1983.

[50] S. F. Cogan, "*In vivo* and *in vitro* differences in the charge-injection and electrochemical properties of iridium oxide electrodes," *Conf Proc IEEE Eng Med Biol Soc,* vol. 1, pp. 882-5, 2006.

[51] X. Beebe, and T. L. Rose, "Charge injection limits of activated iridium oxide electrodes with 0.2 ms pulses in bicarbonate buffered saline," *IEEE Trans Biomed Eng,* vol. 35, no. 6, pp. 494-5, Jun, 1988.

[52] D. C. Rodger, A. J. Fong, W. Li, H. Ameri, A. K. Ahuja, C. Gutierrez, I. Lavrov, H. Zhong, P. R. Menon, E. Meng, J. W. Burdick, R. R. Roy, V. R. Edgerton, J. D. Weiland, M. S. Humayun, and Y.-C. Tai, "Flexible parylene-based multielectrode array technology for high-density neural stimulation and recording," *Sensors and Actuators B-Chemical,* vol. 132, pp. 449-460, 2008.

[53] J. D. Weiland, S. Cogan, and M. S. Humayun, "Micro-machined, polyimide stimulating electrodes with electroplated iridium oxide," *Proceedings of the first joint BMES/EMBS Conference*, pp. 378, 1999.

[54] S. Corbett, J. Ketterl, and T. Johnson, "Polymer-Based Microelectrode Arrays," *Materials Research Society Symposium Proceedings,* vol. 926, 2006.

[55] R. D. Meyer, S. F. Cogan, T. H. Nguyen, and R. D. Rauh, "Electrodeposited iridium oxide for neural stimulation and recording electrodes," *IEEE Trans Neural Syst Rehabil Eng,* vol. 9, no. 1, pp. 2-11, Mar, 2001.

[56] K. Yamanaka, "Anodically Electrodeposited Iridium Oxide Films (AEIROF) from Alkaline Solutions," *Japanese Journal of Applied Physics,* vol. 28, no. 4, pp. 632-637, 1989.

[57] S. A. Marzouk, S. Ufer, R. P. Buck, T. A. Johnson, L. A. Dunlap, and W. E. Cascio, "Electrodeposited iridium oxide pH electrode for measurement of extracellular myocardial acidosis during acute ischemia," *Anal Chem,* vol. 70, no. 23, pp. 5054-61, Dec 01, 1998.

[58] E. Slavcheva, R. Vitushinsky, W. Mokwa, and U. Schnakenberg, "Sputtered Iridium Oxide Films as Charge Injection Material for Functional Electrostimulation," *Journal of The Electrochemical Society,* vol. 151, no. 7, pp. E226-E237, 2004.

[59] R. H. Horng, D. S. Wuu, L.H. Wu, and M.K. Lee, "Formation process and material properties of reactive sputtered IrO_2 thin films," *Thin Solid Films,* vol. 373, pp. 231-234, 2000.

[60] T. J. Park, D. S. Jeong, C. S. Hwang, M. S. Park, and N.-S. Kang, "Fabrication of ultrathin IrO_2 top electrode for improving thermal stability of metal–insulator–metal field emission cathodes," *Thin Solid Films,* vol. 471, pp. 236-242, 2005.

[61] A. de Oliveira-Sousa, M. A. S. da Silva, S.A.S. Machado, L.A. Avaca, and P. de Lima-Neto, "Influence of the preparation method on the morphological and electrochemical properties of Ti/IrO_2-coated electrodes," *Electrochimica Acta,* vol. 45, pp. 4467-4473, 2000.

[62] S. J. Cruikshank, T. J. Lewis, and B. W. Connors, "Synaptic basis for intense thalamocortical activation of feedforward inhibitory cells in neocortex," *Nat Neurosci,* vol. 10, no. 4, pp. 462-8, Apr, 2007.

[63] H. S. Mayberg, A. M. Lozano, V. Voon, H. E. McNeely, D. Seminowicz, C. Hamani, J. M. Schwalb, and S. H. Kennedy, "Deep brain stimulation for treatment-resistant depression," *Neuron,* vol. 45, no. 5, pp. 651-60, Mar 03, 2005.

[64] P. Blomstedt, and M. I. Hariz, "Hardware-related complications of deep brain stimulation: a ten year experience," *Acta Neurochir (Wien),* vol. 147, no. 10, pp. 1061-4; discussion 1064, Oct, 2005.

[65] E. S. Boyden, F. Zhang, E. Bamberg, G. Nagel, and K. Deisseroth, "Millisecond-

timescale, genetically targeted optical control of neural activity," *Nat Neurosci,* vol. 8, no. 9, pp. 1263-8, Sep, 2005.

[66] P. Anikeeva, A. S. Andalman, I. Witten, M. Warden, I. Goshen, L. Grosenick, L. A. Gunaydin, L. M. Frank, and K. Deisseroth, "Optetrode: a multichannel readout for optogenetic control in freely moving mice," *Nat Neurosci,* vol. 15, no. 1, pp. 163-70, Dec 04, 2011.

[67] J. Voigts, J. H. Siegle, D. L. Pritchett, and C. I. Moore, "The flexDrive: an ultra-light implant for optical control and highly parallel chronic recording of neuronal ensembles in freely moving mice," *Front Syst Neurosci,* vol. 7, pp. 8, 2013.

[68] S. Royer, B. V. Zemelman, M. Barbic, A. Losonczy, G. Buzsaki, and J. C. Magee, "Multi-array silicon probes with integrated optical fibers: light-assisted perturbation and recording of local neural circuits in the behaving animal," *Eur J Neurosci,* vol. 31, no. 12, pp. 2279-91, Jun, 2010.

[69] F. Pisanello, L. Sileo, I. A. Oldenburg, M. Pisanello, L. Martiradonna, J. A. Assad, B. L. Sabatini, and M. De Vittorio, "Multipoint-emitting optical fibers for spatially addressable *in vivo* optogenetics," *Neuron,* vol. 82, no. 6, pp. 1245-54, Jun 18, 2014.

[70] F. Wu, E. Stark, M. Im, I. J. Cho, E. S. Yoon, G. Buzsaki, K. D. Wise, and E. Yoon, "An implantable neural probe with monolithically integrated dielectric waveguide and recording electrodes for optogenetics applications," *J Neural Eng,* vol. 10, no. 5, pp. 056012, Oct, 2013.

[71] Y. Son, H. J. Lee, J. Kim, H. Shin, N. Choi, C. J. Lee, E. S. Yoon, E. Yoon, K. D. Wise, T. G. Kim, and I. J. Cho, "*In vivo* optical modulation of neural signals using monolithically integrated two-dimensional neural probe arrays," *Sci Rep,* vol. 5, pp. 15466, Oct 23, 2015.

[72] K. Kampasi, E. Stark, J. Seymour, K. Na, H. G. Winful, G. Buzsaki, K. D. Wise, and E. Yoon, "Fiberless multicolor neural optoelectrode for *in vivo* circuit analysis," *Sci Rep,* vol. 6, pp. 30961, Aug 03, 2016.

[73] X. F. Wang, J. Engel, and C. Liu, "Liquid crystal polymer (LCP) for MEMS: processes and applications," *Journal of Micromechanics and Microengineering,* vol. 13, no. 5, pp. 628-633, Sep, 2003.

[74] C. J. Lee, S. J. Oh, J. K. Song, and S. J. Kim, "Neural signal recording using microelectrode arrays fabricated on liquid crystal polymer material," *Materials Science & Engineering C-Biomimetic and Supramolecular Systems,* vol. 24, no. 1-

2, pp. 265-268, Jan 5, 2004.

[75] S. W. Lee, K. S. Min, J. Jeong, J. Kim, and S. J. Kim, "Monolithic Encapsulation of Implantable Neuroprosthetic Devices Using Liquid Crystal Polymers," *Ieee Transactions on Biomedical Engineering,* vol. 58, no. 8, Aug, 2011.

[76] C. Hassler, T. Boretius, and T. Stieglitz, "Polymers for Neural Implants," *Journal of Polymer Science Part B-Polymer Physics,* vol. 49, no. 1, pp. 18-33, Jan 1, 2011.

[77] T. M. Gwon, J. H. Kim, G. J. Choi, and S. J. Kim, "Mechanical interlocking to improve metalpolymer adhesion in polymer-based neural electrodes and its impact on device reliability," *Journal of Material Science,* vol. 51, no. 14, pp. 6897-6912, 2016.

[78] K. S. Min, C. J. Lee, S. B. Jun, J. Kim, S. E. Lee, J. Shin, J. W. Chang, and S. J. Kim, "A liquid crystal polymer-based neuromodulation system: an application on animal model of neuropathic pain," *Neuromodulation,* vol. 17, no. 2, pp. 160-9, Feb, 2014.

[79] S. Shin, J. Kim, J. Jeong, T. M. Gwon, G. J. Choi, S. E. Lee, J. Kim, S. B. Jun, J. W. Chang, and S. J. Kim, "High Charge Storage Capacity Electrodeposited Iridium Oxide Film on Liquid Crystal Polymer-Based Neural Electrodes," *Sensors and Materials,* vol. 28, no. 3, pp. 243-260, 2016.

[80] J. Jeong, S. W. Lee, K. S. Min, S. Shin, S. B. Jun, and S. J. Kim, "Liquid Crystal Polymer(LCP), an Attractive Substrate for Retinal Implant," *Sensors and Materials,* vol. 24, no. 4, pp. 189-203, Jan 1, 2012.

[81] J. Jeong, S. H. Bae, K. S. Min, J. M. Seo, H. Chung, and S. J. Kim, "A Miniaturized, Eye-Conformable, and Long-Term Reliable Retinal Prosthesis Using Monolithic Fabrication of Liquid Crystal Polymer (LCP)," *Ieee Transactions on Biomedical Engineering,* vol. 62, no. 3, pp. 982-989, Mar, 2015.

[82] T. M. Gwon, K. S. Min, J. H. Kim, S. H. Oh, H. S. Lee, M. H. Park, and S. J. Kim, "Fabrication and evaluation of an improved polymer-based cochlear electrode array for atraumatic insertion," *Biomedical Microdevices,* vol. 17, no. 2, Apr, 2015.

[83] J. H. Kim, K. S. Min, S. K. An, J. S. Jeong, S. B. Jun, M. H. Cho, Y. D. Son, Z. H. Cho, and S. J. Kim, "Magnetic Resonance Imaging Compatibility of the Polymer-based Cochlear Implant," *Clin Exp Otorhinolaryngol,* vol. 5 Suppl 1, pp. S19-23, Apr, 2012.

[84] D. Ha, W. N. de Vries, S. W. M. John, P. P. Irazoqui, and W. J. Chappell, "Polymer-based miniature flexible capacitive pressure sensor for intraocular

pressure (IOP) monitoring inside a mouse eye," *Biomedical Microdevices,* vol. 14, pp. 207-215, 2012.

[85] J. Jeong, S. W. Lee, K. S. Min, and S. J. Kim, "A novel multilayered planar coil based on biocompatible liquid crystal polymer for chronic implantation," *Sensors and Actuators a-Physical,* vol. 197, pp. 38-46, Aug 1, 2013.

[86] Y. Qin, M. M. R. Howlader, M. J. Deen, Y. M. Haddara, and P. R. Selvaganapathy, "Polymer integration for packaging of implantable sensors," *Sensors and Actuators B-Chemical,* vol. 202, pp. 758-778, 2014.

[87] A. J. T. Teo, A. Mishra, I. Park, Y.-J. Kim, W.-T. Park, and Y.-J. Yoon, "Polymeric Biomaterials for Medical Implants and Devices," *ACS Biomaterials Science & Engineering,* vol. 2, pp. 454-472, 2016.

[88] N. Inagaki, "Role of polymer chain end groups in plasma modification for surfacemetallization of polymericmaterials," *Polymer International,* vol. 58, pp. 585-593, 2009.

[89] R. N. Dean, J. Weller, M. J. M. J. Bozack, C. L. Rodekohr, B. Farrell, L. Jauniskis, J. Ting, D. J. Edell, and J. F. Hetke, "Realization of Ultra Fine Pitch Traces on LCP Substrates," *IEEE TRANSACTIONS ON COMPONENTS AND PACKAGING TECHNOLOGIES,* vol. 31, no. 2, pp. 315-321, 2008.

[90] F. Robicsek, J. P. Rielly, and M.-C. Marroum, "The Use of Cyanoacrylate Adhesive (Krazy Glue) in Cardiac Surgery," *Journal of Cardia Surgery,* vol. 9, pp. 353-356, 1994.

[91] P. A. KASELOO, A. H. WEATHERLEY, J. L OTIMER, and M. D. FARINA, "A biotelemetry system recording fish activity," *Journal of Fish Biology,* vol. 40, pp. 165-179, 1992.

[92] S. BHENDE, S. ROTHENBURGER, D. J. SPANGLER, and M. DITO, "*In Vitro* Assessment of Microbial Barrier Properties of Dermabond® Topical Skin Adhesive," *Surgical Infections,* vol. 3, no. 3, pp. 251-257, 2002.

[93] Y. J. Lee, G. B. Jung, S. Choi, G. Lee, J. H. Kim, H. S. Son, H. Bae, and H. K. Park, "Biocompatibility of a novel cyanoacrylate based tissue adhesive: cytotoxicity and biochemical property evaluation," *PLoS One,* vol. 8, no. 11, pp. e79761, 2013.

[94] G. Hernandez, S. Hamdani, H. Rajabi, K. Conover, J. Stewart, A. Arvanitogiannis, and P. Shizgal, "Prolonged rewarding stimulation of the rat medial forebrain bundle: neurochemical and behavioral consequences," *Behav. Neurosci.*, vol. 120,

no. 4, pp. 888-904, 2006.

[95] S. K. Talwar, S. Xu, E. S. Hawley, S. A. Weiss, K. A. Moxon, and J. K. Chapin, "Rat navigation guided by remote control," *Nature,* vol. 417, no. 6884, pp. 37-8, May 02, 2002.

[96] M.-G. Lee, G. Jun, H.-S. Choi, H. S. Jang, Y. C. Bae, K. Suk, I.-S. Jang, and B.-J. Choi, "Operant conditioning of rat navigation using electrical stimulation for directional cues and rewards," *Behavioural Processes,* vol. 84, pp. 715-720, 2010.

[97] J. Kim, J. Kim, K. S. Min, S. E. Lee, S. J. Kim, and J. W. Chang, "VPL-DBS on neuropathic pain rat model is effective in mechanical allodynia than cold allodynia," *Neurological Sciences,* vol. 33, pp. 1265-1270, 2012.

[98] J. Kim, S. E. Lee, J. Shin, H. H. Jung, S. J. Kim, and J. W. Chang, "The Neuromodulation of Neuropathic Pain by Measuring Pain Response Rate and Pain Response Duration in Animal," *Journal of Korean Neurosurgical Society,* vol. 57, no. 1, pp. 6-11, 2015.

[99] M. H. Zimmermann: Xylem Structure and the Ascent of Sap. (Springer-Verlag, Berlin-Heidelberg-New York-Tokyo 1983) p. 143.

[100] G. Paxinos and C. Watson: The rat brain in stereotaxic coordinates, (Academic Press, San Diego, 1998)

[101] B. H. Lee, R. Won, E. J. Baik, S. H. Lee, and C. H. Moon, "An animal model of neuropathic pain employing injury to the sciatic nerve branches," *Neuroreport,* vol. 11, no. 4, pp. 657-661, 2000.

[102] J. M. Lucas, Y. Ji, and R. Masri, "Motor cortex stimulation reduces hyperalgesia in an animal model of central pain," *Pain,* vol. 152, no. 6, pp. 1398-407, Jun, 2011.

[103] W. F. Agnew and D. B. McCreery, Neural Prostheses: Fundamental Studies. Englewood Cliffs, NJ: Prentice-Hall, 1990.

[104] C. M. Lopez, A. Andrei, S. Mitra, M. Welkenhuysen, W. Eberle, C. Bartic, R. Puers, R. F. Yazicioglu, and G. G. E. Gielen, "An Implantable 455-Active-Electrode 52-Channel CMOS Neural Probe," *IEEE JOURNAL OF SOLID-STATE CIRCUITS*, vol. 49, no. 1, pp.248-261, 2014.

[105] G. Buzsaki, "Large-scale recording of neuronal ensembles," *Nat. Neurosci.*, vol. 7, no. 5, pp. 446–451, May 2004.

국문 초록

4면 전극 사이트 (four-sided electrode site)를 갖는 새로운 액정 폴리머 (liquid crystal polymer, LCP) 기반의 신경 프로브 (neural probe)를 개발하고 그 성능을 검증하였다. 신경 프로브는 3-D 신경 회로를 기록하기 위해 3 차원 구성의 채널 (channel)을 갖는 것이 이상적이다. 이와 같은 이유로 지난 수 십 년 동안 많은 종류의 3 차원 신경 프로브가 개발되어왔다. 하지만 대부분의 전극들은 전극 생크 (shank)의 한쪽 면에만 전극 사이트 (electrode site)들이 위치하게 제작되어왔다. 본 논문에서 제안한 액정폴리머 기반의 신경 프로브는 생크의 4개의 측면, 즉 앞면, 뒷면, 두 개의 측면에 모두 전극 사이트가 위치하도록 제작되었다. 이와 같은 구조의 신경 프로브를 제작하기 위해서 다층의 액정 폴리머 필름들의 열압착공정 (thermal lamination)과 레이저 미세 공정 (laser micromachining)이 사용되었다. 제안 된 액정폴리머 기반의 4면 신경 프로브 (four-sided neural probe)를 사용하여, 실험 동물의 일차 체성 감각 피질 (primary somatosensory cortex) 에서 생체 내 다중 채널 신경 기록이 성공적으로 수행되었다. 다중 채널 신경 기록 실험 결과 제안된 4면 신경 프로브가 생크의 한 면에만 위치한 전극들을 갖는 단면 신경 프로브 (single-sided neural probe)에 비해 다양한 세포의 신호들을 기록할 수 있음을 확인하였다. 이와 같은 결과는 두 신경 프로브를 통해 기록된 신경신호들을 피어슨 상관 계수 (Pearson's correlation coefficient) 분석과 교차 상관 (cross-correlation) 분석을 통해서도 증

명되었다.

본 논문에서는 또한 전착 산화 이리듐 막 (electrodeposited iridium oxide film, EIROF)을 사용하여 높은 전하 저장 용량 (charge storage capacity)을 갖는 액정폴리머 기반 자극 전극 (stimulation electrode)을 개발하였다. 액정폴리머 기반의 자극 전극을 제작하여 자극 전극의 사이트에 산화 이리듐을 전착 (electrodeposition)시킴으로써 전하 저장 용량을 증가시켰다. 상이한 수의 직사각형 전압 펄스 및 삼각형 파형을 사용하여 이리듐 산화물을 전착한 후 전기 화학적 임피던스 (electrochemical impedance)와 전하 저장 용량을 측정하여 전기화학적 특성을 분석하였다. 또한 전착한 산화 이리듐의 표면을 원자력 현미경 (atomic force microscopy, AFM)과 주사 전자 현미경 (scanning electron microscopy, SEM)을 이용하여 측정 및 분석하였다. 추가적으로 산화 이리듐의 표면의 물질 조성을 X 선 광전자 분광법 (X-ray photoelectron spectroscopy, XPS)을 이용하여 정량적으로 측정하였다. 마지막으로, 전착 산화 이리듐 막의 신경 자극 전극으로써의 성능을 확인하기 위해 실험 동물에서의 생체 내 신경 자극 실험을 수행하였다.

광학 자극 (light stimulation, optical stimulation)과 전기적 기록 (electrical recording)을 할 수 있는 액정폴리머 기반의 옵트로드 (optrode) 또한 본 논문에서 제안한다. 제안된 옵트로드는 전극의 생크의 팁 (tip)에 4개의 기록 채널 (recording channel)을 갖도록 디자인 되었다. 이와 같은 구조의 신경 전극은 다층의 액정폴리머 필름들을 열압착한 후 레이저 이용하여 전기 도금 (electroplated) 된 금속의 잘린 단

면을 기록 전극 사이트로 사용하도록 제작 된다. 팁에 위치한 4개의 기록 전극은 팁에 위치한 구조적 특징 덕분에 신경 신호 기록에 유리한 구조를 갖고 있다는 장점이 있다. 제작된 신경 신호 기록 전극 사이트들은 신경 신호 기록의 양호한 품질을 보장하기에 충분한 접촉 영역 및 전기화학적 임피던스를 갖는 것을 확인하였다. 이와 같이 레이저 절단 과정을 거쳐 제작된 신경 전극에 광섬유 (optic fiber)를 연결하여 옵트로드를 제작한다. 제작 된 액정폴리머 기반의 옵트로드의 광학 자극 및 전기적 신경 신호 기록의 성능을 확인하기 위해 실험동물의 생체 내 실험이 수행하였다. 그 결과, 제작된 옵트로드를 사용하여 자발적 신경 신호 (spontaneous activity)와 광 유발 신경 신호 (light-evoked activity)가 실험동물의 피질 (cortex)과 심부 뇌 영역 (deep brain area)에서 모두 성공적으로 기록되는 것을 확인할 수 있었다.

주요어: 신경전극, 액정폴리머, 3차원, 테트로드, 옵트로드, 기록전극, 자극전극, 이리듐 옥사이드

학 번: 2013-30244